Structural Studies of the Sterol Transporter ABCG5/G8: Nanodisc Reconstitution, Cryo-EM, and Nanobody Discovery

Gonca Gursu

Thesis submitted to the University of Ottawa
in partial fulfillment of the requirements for the
Master of Science in Microbiology and Immunology

Department of Biochemistry, Microbiology and Immunology

Faculty of Medicine
University of Ottawa

Abstract

ABCG5/G8 is a heterodimeric ATP binding cassette transporter that mediates cholesterol and dietary plant sterol efflux in the liver and intestine and plays an essential role in sterol homeostasis. Dysfunction of ABCG5/G8 is associated with sitosterolemia and cardiovascular disease risk. Despite progress in structural characterization, available structures have been determined in detergent micelles or restricted lipid environments which may not accurately reflect the native membrane context. In this thesis, ABCG5/G8 was expressed in *Pichia pastoris*, purified, and reconstituted into lipid nanodiscs by evaluating four membrane scaffold protein and lipid combinations. The optimal MSP1E3D1/POPC condition enabled single particle cryo-EM structure determination in a native-like lipid bilayer environment under apo, cholesterol-incubated, and cholesterol/AMP-PNP-incubated conditions, with the apo reconstruction reaching 3.15 Å resolution. In parallel, five unique ABCG5/G8 binding nanobodies were identified using yeast surface display. Together, this work establishes a foundation for structural studies of ABCG5/G8 in a native-like lipid bilayer environment and provides ABCG5/G8 specific nanobodies as new molecular tools for future structural and therapeutic applications.

Acknowledgments

First and foremost, I want to thank my supervisor, Dr. Jyh-Yeuan Lee, for his continuous support throughout this entire journey. Thank you for your patience, motivation, and for generously sharing your immense knowledge with me. I am truly grateful that you entrusted me with such an exciting project and for the way you have consistently encouraged me to pursue my scientific career with curiosity and enthusiasm.

I sincerely thank my committee members, Dr. Patrick Giguère and Dr. Joey Sheff, who have provided me with invaluable suggestions, insightful feedback, and constant encouragement throughout my studies. I am particularly grateful to Dr. Giguère for his generosity with his time and willingness to meet with me whenever I needed guidance.

A very special thanks goes to all the members of the Lee Lab for their invaluable advice and unwavering support, especially Kadambari Vijay Sai and Fatemeh Rezaei, whose help have made this experience truly memorable.

I would also like to thank Dr. Di Wu for generously granting us access to the cryo-EM facility at the Max Planck Institute in Frankfurt, for establishing this collaboration, and for being a wonderful mentor whose expertise and guidance have been deeply appreciated.

Finally, I am grateful to my family and friends for their unconditional love, patience, and encouragement, without which none of this would have been possible.

Contribution of Authors

Gonca Gursu[1], Jyh-Yeuan Lee[1]*
[1][Department of Biochemistry, Microbiology and Immunology, University of Ottawa, Ottawa, ON, Canada, K1N 6N5]
*Corresponding Author

This thesis was written by Gonca Gursu. All experiments, data analysis, figure preparation, and writing were performed by the author unless otherwise specified. The study was designed and supervised by Dr. Jyh-Yeuan Lee.

Membrane Scaffold Proteins

Dr. Bala Xavier contributed to the establishment of the membrane scaffold protein (MSP) expression and purification protocols.

Cryo-EM Data Collection and Processing

Haoran Fu, under the supervision of Dr. Di Wu at MPI-Biophysics, collected and processed the cryo-EM data.

Thermal Stability Measurements

Sophie Wen (laboratory of Dr. Jamshid Tanha at NRC) performed the differential scanning fluorimetry (DSF) measurements.

Thesis Supervision

Dr. Jyh-Yeuan Lee (Department of Biochemistry, Microbiology and Immunology, University of Ottawa) supervised all stages of the project, contributed to experimental design and interpretation, and provided feedback on all written chapters.

Abbreviations

Abbreviation	Definition
ABC	ATP-binding cassette
AMP-PNP	Adenylyl-imidodiphosphate
ATP	Adenosine triphosphate
BCA	Bicinchoninic acid
BSA	Bovine serum albumin
CDR	Complementarity-determining region
CHS	Cholesteryl hemisuccinate
CoA	Coenzyme A
Cryo-EM	Cryo electron microscopy
CTF	Contrast transfer function
CV	Column volume
DDM	n-Dodecyl-β-D-maltoside
DMSO	Dimethyl sulfoxide
DNA	Deoxyribonucleic acid
DSF	Differential scanning fluorimetry
ECD	Extracellular domain
EDTA	Ethylenediaminetetraacetic acid
EGTA	Ethylene glycol-bis(β-aminoethyl ether)-N,N,N′,N′-tetraacetic acid
E. coli	Escherichia coli
FPLC	Fast protein liquid chromatography
FSC	Fourier shell correlation
HCAb	Heavy-chain only antibody
HCl	Hydrochloric acid
HDL	High-density lipoprotein

Abbreviation	Definition
IPTG	Isopropyl β-D-1-thiogalactopyranoside
LB	Luria-Bertani
LDL	Low-density lipoprotein
MD	Minimal dextrose
MDR	Multidrug resistance
MGY	Minimal glycerol yeast
MSP	Membrane scaffold protein
Nb	Nanobody
NBD	Nucleotide binding domain
Ni-NTA	Nickel-nitrilotriacetic acid
PCR	Polymerase chain reaction
PDB	Protein Data Bank
PMSF	Phenylmethylsulfonyl fluoride
POPC	1-Palmitoyl-2-oleoyl-sn-glycero-3-phosphocholine
POPE	1-Palmitoyl-2-oleoyl-sn-glycero-3-phosphoethanolamine
RCT	Reverse cholesterol transport
SDS-PAGE	Sodium dodecyl sulfate–polyacrylamide gel electrophoresis
SEC	Size-exclusion chromatography
TB	Terrific broth
TICE	Trans intestinal cholesterol efflux
TMD	Transmembrane domain
VHH	Variable heavy domain of heavy-chain only antibody (nanobody)
YNB	Yeast nitrogen base

Table of Contents

List of Figures

List of Tables

1. Introduction

1.1. Cholesterol Metabolism and Homeostasis

Cholesterol is an essential component of cell membranes in vertebrates, where it can account for a substantial portion of the membrane lipids, reported at up to around 40 mol %, however the exact value varies between cell types and between the two membrane leaflets[1]. In addition to contributing to membrane architecture, cholesterol regulates membrane fluidity and integrity, by inserting itself between phospholipid molecules and modulating their packing[2]. Cholesterol serves as the precursor for steroid hormones, which act as crucial regulators in various metabolic pathways and modulate gene expression[3]. In cell membranes, cholesterol is a key component of lipid rafts; small, dynamic membrane regions enriched in cholesterol and sphingolipids. These rafts contribute to processes such as membrane signaling and trafficking[4]. Additionally, cholesterol is the precursor of bile acids, which facilitate the absorption of dietary lipids and nutrients in the small intestine[5]. Sterols are poorly soluble in the aqueous intestinal lumen, so bile acids and phospholipids solubilize them into mixed micelles, which deliver sterols to the enterocyte surface. The subsequent absorption of these sterols is tightly controlled by dedicated sterol-transport proteins, as a key gatekeeping system by exporting cholesterol and especially plant sterols back into the intestinal lumen, thereby limiting their net absorption[6]. Disrupted cholesterol metabolism contributes to major cardiovascular and metabolic diseases, especially atherosclerosis, while elevated plasma cholesterol remains an important risk factor for cardiovascular disease[7].

Cholesterol lowering therapies primarily act by reducing cholesterol synthesis or increasing low-density lipoprotein (LDL) clearance. Statins inhibit HMG-CoA reductase, whereas therapies

targeting PCSK9 increase hepatic LDL-receptor availability and enhance removal of LDL-cholesterol from the circulation[8,9]. A newer agent, bempedoic acid, extends these approaches by inhibiting ATP-citrate lyase and has been shown to reduce cardiovascular events in statin-intolerant patients[10]. Despite these advances, many patients still require additional lipid-lowering therapy to reach recommended LDL targets[11], demonstrating the need for complementary strategies, including approaches that improve sterol elimination in the guts. Cholesterol is obtained through two principal routes: *de novo* biosynthesis from acetyl-CoA or dietary uptake in the gut. In addition to cholesterol, the human diet provides a significant number of structurally related plant sterols (phytosterols), such as campesterol, stigmasterol, and sitosterol, which are consumed in amounts roughly equivalent to dietary cholesterol[12,13]. If not removed, the accumulation of phytosterol becomes toxic to cells, disturbs lipid metabolism, and contributes to hyperlipidemia, a significant risk factor leading to cardiovascular diseases and metabolic disorders[14].

While mammalian cells have the capability to synthesize cholesterol, the majority lack the ability to metabolize it. Therefore, excess cholesterol needs to be either exported from the cell or stored as cholesteryl esters. It is ultimately transported to the liver for elimination through bile and the intestine, making sterol export essential for maintaining whole-body cholesterol balance[15]. Since not all imported cholesterol is metabolized within the cells, excess free cholesterol must be removed from the body through two metabolic pathways: trans-intestinal cholesterol efflux (TICE) and reverse cholesterol transport (RCT)[16,17]. In RCT, excess cholesterol from peripheral tissues is transported to the liver via high-density lipoprotein (HDL) particles, for excretion in the bile or conversion to the bile acids before excretion[18]. While in TICE, cholesterol is directly transported into the intestinal lumen via the enterocytes for fecal elimination, and it was shown to contribute ~30% of total fecal cholesterol excretion in mice[19] and was later shown in humans as well[20]. The

movement of cholesterol molecules across cellular membranes thus plays an essential role in these pathways[21], which are heavily driven by lipid transport membrane proteins that are associated with phospholipid or sterol transport to maintain lipid homeostasis[14,22].

1.2. ATP-binding cassette (ABC) Transporters

The ABC transporter superfamily contributes to maintaining lipid homeostasis by transporting lipid substrates across cellular membrane utilizing ATP hydrolysis[23]. ABC transporters can be broadly categorized as importers or exporters, based on their direction of substrate transport. Exporters mediate the efflux of molecules from the cytoplasm to the extracellular space or into intracellular organelles, while importers control the amount of essential nutrients that enter cells[24]. All ABC transporters share a conserved structural framework including two nucleotide binding domains (NBDs) that are located in the cytoplasm and hydrolyze ATP to provide the energy required for substrate transport, and two transmembrane domains (TMDs) embedded in the membrane, which form the substrate translocation pathway and regulate transporter activity[25].

Human ABC proteins are divided into seven subfamilies, ranging from ABCA to ABCG, according to similarities in the gene and amino acid sequences as well as the structural topology[26] **(Figure 1.1)**. Members of each subfamily have different physiological roles and substrate specificities, ranging from the export of drugs and xenobiotics to the transport of lipids and sterols[23]. Among these are members from the ABCG subfamily: ABCG1, ABCG4, ABCG5, and ABCG8, which are associated with lipid and cholesterol metabolism, while ABCG2 mediates efflux of uric acid or polycyclic drugs. ABCG2 is expressed in a wide range of tissues and contributes to multidrug resistance (MDR) in cancer chemotherapy[27]. ABCG1 and ABCG4 play

important roles in maintaining cholesterol homeostasis in the brain and macrophage rich tissues[28] whereas ABCG5 and ABCG8 are responsible for the elimination of cholesterol and dietary plant sterols at the liver and small intestine[29].

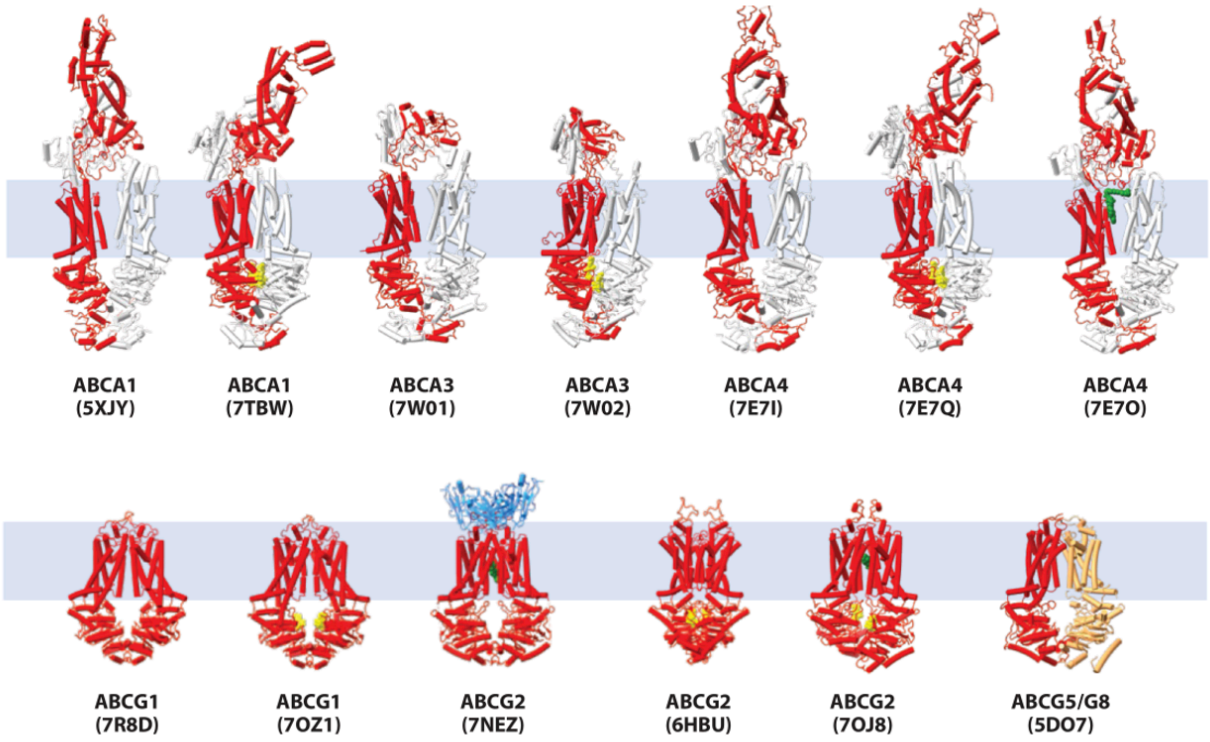

Figure 1.1. Representative structures of type II human ABC transporters.
Experimentally determined structures of selected type II human ABC transporters from the ABCA and ABCG subfamilies are shown, including ABCA1, ABCA3, ABCA4, ABCG1, ABCG2, and ABCG5/G8. These structures illustrate the overall architecture of type II ABC transporters and show differences between the ABCA and ABCG subfamilies. Figure adapted from Alam and Locher (2023).

1.3. ABCG5/G8

ABCG5 and ABCG8 are located on chromosome 2p21 and are encoded by two separate genes arranged head-to-head on opposite DNA strands, separated by a short bidirectional promoter, so they are co-regulated and expressed together as a functional unit[30]. Their expression is closely

coordinated and responds to changes in sterol and bile acid metabolism. Several transcription factors contribute to this regulation, including HNF4α, GATA4, GATA6, and LRH-1, which binds within the intergenic promoter region[31,32]. Liver X receptors, LXRα and LXRβ, help the body respond to changes in sterol levels. As intracellular cholesterol increases, oxysterols activate LXR, which promotes ABCG5 and ABCG8 transcription and thereby increases the capacity for sterol elimination[33]. Post-transcriptional regulation is essential, as proper maturation and trafficking are necessary for the formation of a functional ABCG5/G8 heterodimer. Both subunits undergo N-glycosylation within their extracellular domains: ABCG5 at Asn585 and Asn592, and ABCG8 at Asn619. These modifications facilitate correct protein folding and enable escape from the endoplasmic reticulum[34]. Collectively, transcriptional and post-translational mechanisms regulate ABCG5/G8 abundance in response to sterol availability and ensure that only properly assembled transporters are delivered to the membrane.

ABCG5/G8 **(Figure 1.2)**, a heterodimeric transporter formed by the obligate interaction of two closely related ABC proteins, ABCG5 and ABCG8, is responsible for clearing excess cholesterol and dietary plant sterols from the body[35,36]. It is predominantly expressed in the hepatocytes and enterocytes, where it localizes to the canalicular membrane and mediates the efflux of sterol molecules into the bile and the lumen of the small intestine, respectively[29]. By being expressed at both the liver and intestine, ABCG5/G8 plays a significant role in the biliary and trans intestinal cholesterol elimination pathways, preventing the accumulation of excess cholesterol and dietary plant sterols and maintaining sterol balance in the body[27]. ABCG5/G8 is a sterol selective transporter whose principal physiological substrates are cholesterol and dietary plant sterols (phytosterols) such as sitosterol, campesterol, and stigmasterol[37] **(Figure 1.3)**. This

selectivity is important for human health, as phytosterols are poorly metabolized by our cells and must be actively excluded from absorption to prevent their accumulation[13].

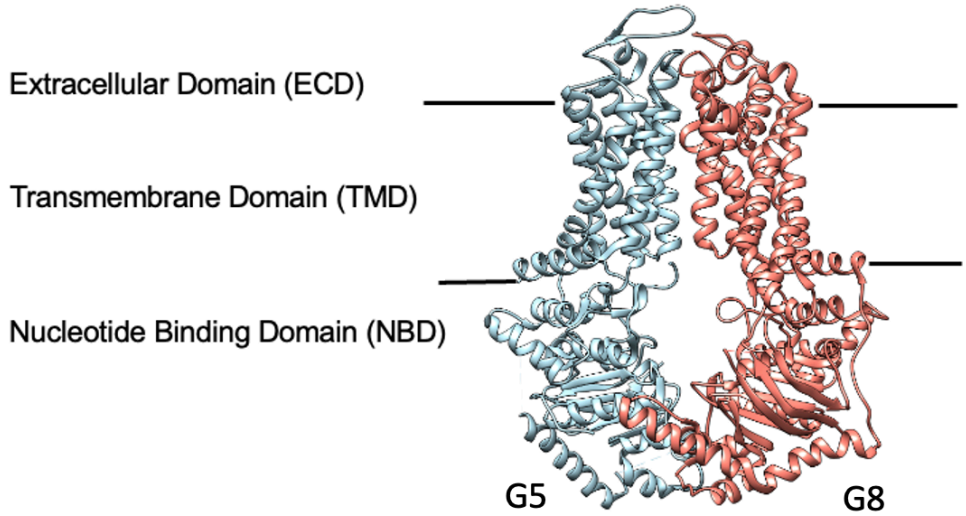

Figure 1.2. Crystal structure of ABCG5/G8 (PDB: 8CUB).
Cartoon representation of ABCG5 (light blue) and ABCG8 (salmon), highlighting the extracellular domain (ECD), transmembrane domain (TMD), and nucleotide binding domain (NBD) of each subunit.

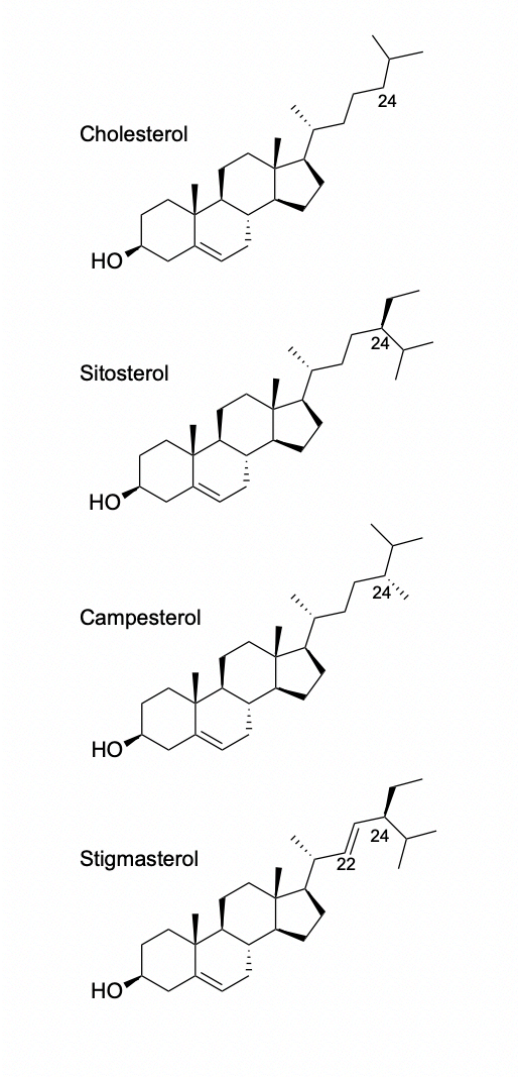

Figure 1.3. Sterol structures of cholesterol and three phytosterols.
Cholesterol, sitosterol, campesterol, and stigmasterol share an identical tetracyclic steroid ring scaffold, with major differences arising from substitutions at carbon 24 (C24) of the side chain. Compared to cholesterol, campesterol carries an additional methyl group at C24, sitosterol has an ethyl group at C24, and stigmasterol contains an ethyl group at C24 along with an additional double bond between C22 and C23. The structures were drawn in ChemDraw using molecular structure data from PubChem.

ABCG5/G8 is important for two major routes of sterol elimination from the body, biliary cholesterol secretion and transintestinal cholesterol efflux (TICE) **(Figure 1.4)**. In hepatocytes, ABCG5/G8 is located on the apical canalicular membrane and actively transports cholesterol and phytosterols from the cytoplasm to the bile canaliculi for excretion in the bile[29]. Mice deficient in

ABCG5/G8 show decreased biliary cholesterol secretion and increased plant sterol accumulation, consistent with the role of this transporter in hepatic sterol secretion[38].

In enterocytes of the small intestine, ABCG5/G8 is located in the apical membrane and mediates efflux of absorbed cholesterol and dietary plant sterols back into the intestinal lumen. Although cholesterol and non-cholesterol foreign sterols (xenosterols) are consumed in roughly equal amounts in a typical diet, only about 5% of xenosterols are absorbed compared to approximately 50% of dietary cholesterol[39]. This selective absorption of cholesterol over xenosterols largely depends on the efflux activity of ABCG5/G8. In addition to regulating dietary sterol absorption, ABCG5/G8 is involved in TICE, a non-biliary pathway in which cholesterol is transported directly from the blood stream through the enterocytes into the intestinal lumen[19]. TICE is an important route for cholesterol homeostasis in humans, corresponding to ~35 % of total fecal cholesterol excretion. In the small intestines, NPC1L1 is a major transporter to uptake dietary sterols; when treated with the NPC1L1 inhibitor ezetimibe, TICE in humans or mouse models was shown active, indicating the cholesterol excretion into the intestinal lumen largely through ABCG5/G8[20]. These results support TICE as a physiologically and potentially therapeutically relevant pathway, distinct from the classical biliary route, that could be targeted to enhance cholesterol elimination in the treatment of cardiovascular disease.

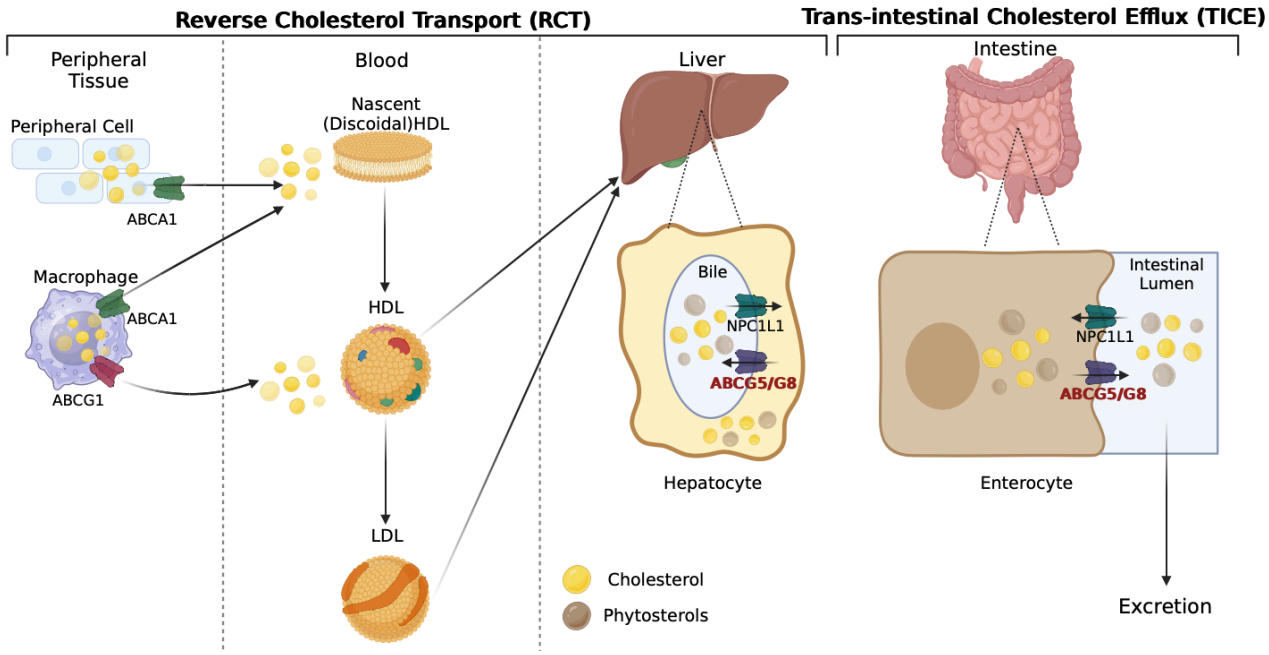

Figure 1.4. Schematic representation of the major cholesterol elimination pathways in humans, reverse cholesterol transport (RCT) and trans intestinal cholesterol efflux (TICE).
In RCT, excess cholesterol from peripheral tissues, including peripheral cells and macrophages, is effluxed into the bloodstream through the action of ABCA1 and ABCG1, where it is loaded onto nascent (discoidal) HDL particles[40]. As HDL particles mature in circulation, they accumulate additional cholesterol and are eventually delivered to the liver, either directly or through the conversion into LDL. In hepatocytes, ABCG5/G8 mediates the efflux of cholesterol and phytosterols into the bile canaliculi for biliary excretion, opposing the cholesterol importer activity of NPC1L1. In the TICE pathway, cholesterol from the bloodstream is transported directly across enterocytes of the small intestine, where ABCG5/G8 secretes cholesterol and phytosterols into the intestinal lumen for fecal excretion, again opposing the import activity of NPC1L1. Cholesterol and phytosterol molecules are represented as yellow and brown circles, respectively. Figure created with BioRender.

1.4. Sitosterolemia

Sitosterolemia is an autosomal recessive disorder caused by loss of function mutations in either the ABCG5 or ABCG8 gene, which disrupt the function of heterodimeric transporter. Since both ABCG5 and ABCG8 are required for the formation of a functional transporter, mutations in either gene result in the same disease phenotype **(Figure 1.5)**[41]. Malfunction of this transporter leads to the accumulation of dietary sterols in the body, as ABCG5/G8 normally limits their absorption in the intestine and mediates their excretion from the liver into the bile[42]. In the absence of functional ABCG5/G8, patients show elevated plasma levels of phytosterols such as sitosterol

and campesterol, often reaching levels 30- to 100-fold higher than in healthy individuals[43]. This progressive accumulation of sterols can result in premature atherosclerosis, a significant risk factor for cardiovascular diseases, such as strokes, which is a leading cause of death globally[44–46]. Additional clinical features include the formation of tendon and tuberous xanthomas, coronary artery disease and hemolytic anemia[13].

Sitosterolemia can look similar to familial hypercholesterolemia (FH) because both may cause hypercholesterolemia, tendon xanthomas, and premature atherosclerosis, so it is often misdiagnosed as FH[47]. The two conditions, however, have different causes. FH happens when the body cannot clear LDL cholesterol properly, most commonly due to loss-of-function variants in LDLR, but also mutations in APOB or in PCSK9, leading to accumulation of LDL-cholesterol in the circulation[48]. Sitosterolemia, on the other hand, is a disorder of sterol absorption and excretion in which loss of ABCG5/G8 increases intestinal uptake and reduces biliary elimination of plant sterols and cholesterol[49]. This difference matters for both diagnosis and treatment. People with sitosterolemia have much higher levels of plant sterols in their blood, which helps tell it apart from FH. FH is usually treated by lowering cholesterol production and helping the body clear LDL, but sitosterolemia does not respond as well to statins. Instead, so far, it is mainly managed by limiting sterols in the diet and using ezetimibe to inhibit sterol uptake in the intestines[50].

Table 1. Comparison of sitosterolemia and familial hypercholesterolemia (FH)[38,50]

Both disorders can present with hypercholesterolemia, xanthomas, and premature coronary disease, but they differ in their underlying mechanism, biochemical features, and response to treatment.

Feature	Familial hypercholesterolemia (FH)	Sitosterolemia
Inheritance	Autosomal dominant	Autosomal recessive
Gene(s) affected	LDLR (most common), APOB, PCSK9	ABCG5 or ABCG8
Primary defect	Impaired LDL-receptor–mediated clearance of circulating LDL	Impaired sterol excretion
Plasma cholesterol	Elevated LDL-cholesterol	Elevated cholesterol variable (can normalize on low-sterol diet)
Plasma phytosterols (sitosterol, campesterol)	Normal	Elevated (~30-100× normal)
Shared clinical features	Tendon xanthomas, premature atherosclerosis / coronary artery disease	Tendon xanthomas, premature atherosclerosis / coronary artery disease also hemolytic anemia
Response to statins	Good (LDL-lowering effective)	Poor
Primary treatment	Statins; ezetimibe and PCSK9 inhibitors as add-on	Dietary sterol (plant-sterol) restriction + ezetimibe

Beyond sitosterolemia, ABCG5/G8 has also been involved in more conditions of cholesterol metabolism. Genetic variants in ABCG5 and ABCG8 have been associated with changes in plasma cholesterol levels, increased risk of gallstone disease, and increased risk of cardiovascular disease[51]. These observations suggest a wider physiological role for ABCG5/G8 and support exploring its potential as a therapeutic target in hypercholesterolemia and related cardiovascular disease. However, specific therapies targeting ABCG5/G8 or ABC cholesterol efflux transporters remain limited. This gap in treatment options presents challenge in managing conditions related to cholesterol metabolism and transport, including sitosterolemia and hypercholesterolemia. Therefore, it is necessary to develop therapeutic drugs that specifically target ABCG5/G8.

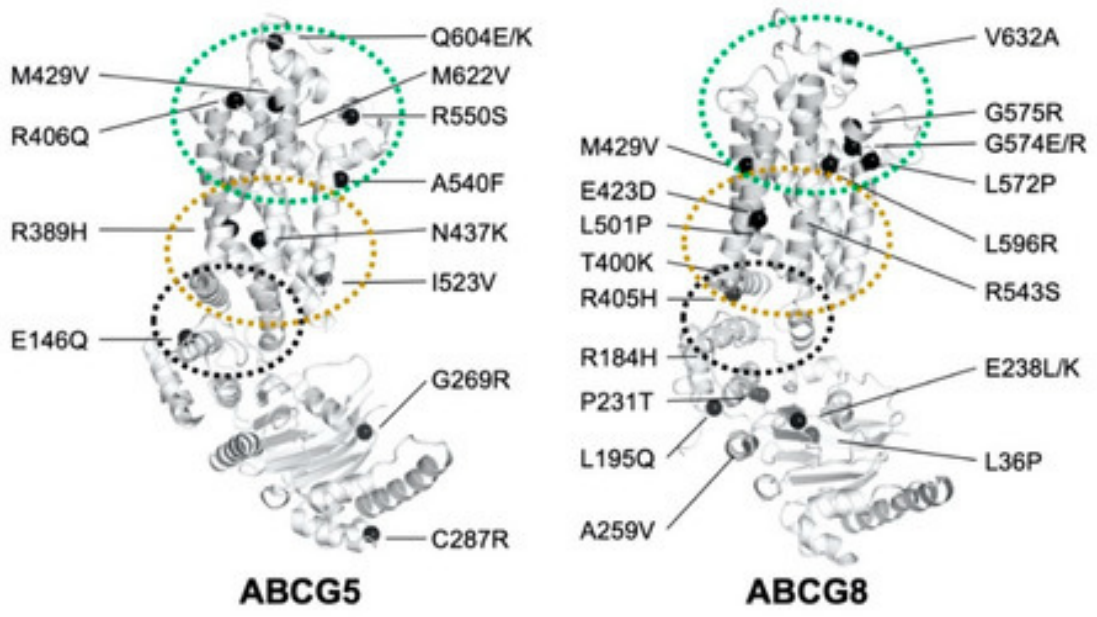

Figure 1.5. Mapping of missense mutations on the ABCG5 and ABCG8 structures.
Disease associated missense mutations identified in patients are shown as black spheres on the crystal structures of ABCG5 (PDB: 5DO7, chain C) and ABCG8 (PDB: 5DO7, chain D). Three structural regions are highlighted by dashed ovals: the triple helical bundle (black), the polar relay within the transmembrane domain (TMD, yellow), and the extracellular domain with its re-entry helices (green). Figure adapted from Xavier et al. (2020).

1.5. Structure of ABCG5/G8

The first structure of human ABCG5/G8 was reported and solved by X-ray crystallography in 2016. This provided the first molecular view of sterol transport by this heterodimeric transporter[35]. The structure was solved in a nucleotide free, inward facing conformation at 3.9 Å resolution and revealed the overall architecture of the heterodimer, including the arrangement of the two TMDs that form the substrate translocation pathway and the two NBDs that drive ATP hydrolysis. This structure identified a polar relay network within the TMDs, which was later shown to play an important role in regulating the ATPase activity and sterol transport function of ABCG5/G8 through analysis of disease causing mutations[52].

In recent years, the progress in single particle cryo-EM has allowed the determination of ABCG5/G8 structures in complex with substrates or modulating ligands. Cryo-EM structure of

ABCG5/G8 was determined at 3.3 Å resolution in complex with Fab fragments of two modulating monoclonal antibodies, revealing a symmetric interface between the two NBDs, stabilized by a network of salt bridges between the conserved NPXDFXXD motifs **(Figure 1.6)**[53].

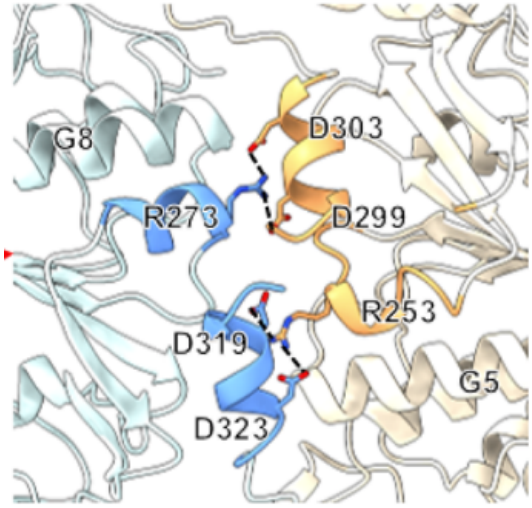

Figure 1.6. Salt bridge network at the NBD dimer interface of ABCG5/G8.
The two aspartate residues at the C-terminus of the short helical NPXDFXXD form pairs of salt bridges with positively charged arginine residues from the opposing half transporter. Specifically, Arg253 of ABCG5 interacts with Asp319 and Asp323 of ABCG8, whereas Arg273 of ABCG8 interacts with Asp299 and Asp303 of ABCG5. Figure adapted from Zhang et al. (2021).

At the same time, cryo-EM and X-ray structures of ABCG5/G8 in the presence of cholesterol identified cholesterol binding pockets in the transmembrane region and provided a molecular basis for cholesterol efflux by ABCG subfamily transporters[36,44]. Together, these structures expanded the structural information available for ABCG5/G8 and provided important insight into its architecture, antibody stabilized NBD interface, and cholesterol binding sites. However, the mechanism of sterol selectivity, the conformational transitions associated with substrate binding and release, and the role of lipid–protein interactions in modulating transporter function remain not fully understood. Native like membrane environment is crucial to answering these questions, which provides a strong rationale for the structural studies described in this thesis.

Table 2. Summary of previously reported ABCG5/G8 structures

Reported structures are summarised by membrane-mimetic environment, ligand condition, and main contribution (PDB codes in parentheses)[35,36,44,53].

Study	Environment	Condition	Main contribution
2016 crystal (5DO7)	DMPC/cholesterol bicelle	Apo / nucleotide-free	First ABCG5/G8 architecture; inward-facing state
2021 cryo-EM (7R8A-B)	Detergent micelle	Sterol-containing	Proposed sterol binding sites and transport mechanism
2021 Fab-bound cryo-EM (7JR7)	Saposin-A nanodisc	Modulating Fabs	Showed Fab-dependent regulation of ATPase activity
2022 crystal (8CUB)	DMPC/cholesterol bicelle	Cholesterol	Provided cholesterol-associated structural information

1.6. Nanodisc Reconstitution

Membrane proteins are a diverse class of proteins essential for various cellular processes, including signal transduction, transport, and catalysis [54]. However, removing membrane proteins from their native cell membranes can be very challenging due to their hydrophobic surfaces, conformational flexibility, and intrinsic lack of stability outside of the lipid bilayer[55]. These properties create difficulties at multiple levels, including expression, solubilization, purification, crystallization, and structure determination[56]. Conventional methods to extract and study

membrane proteins rely on the use of detergents that solubilize the protein in detergent micelles. But detergent micelles often do not fully recreate the native membrane environment and can destabilize membrane proteins leading to loss of activity or aggregation. A potential strategy to overcome these difficulties involves solubilizing and stabilizing membrane proteins within a membrane mimicking environment that resembles a native lipid bilayer[54].

Nanodiscs are self-assembling lipid bilayer particles that provide a soluble and stable surface for solubilizing membrane proteins[57]. This method uses a membrane scaffold protein (MSP), a target protein, and a defined lipid mixture, which spontaneously assemble into discoidal lipid bilayer particles encircled by two copies of MSP. Membrane proteins integrated into these lipid bilayer structures are protected against aggregation and detergent induced destabilization, which frequently complicate structural and functional studies of membrane proteins[58].

The size of nanodiscs can be controlled by varying the length of the MSP, allowing the reconstitution of membrane proteins of different sizes. The original MSP1 construct contains 200 amino acids, and extended variants such as MSP1E1, MSP1E2, and MSP1E3 have been generated by adding 22, 44, and 66 amino acid residues, respectively[59]. The MSP1D1 construct consists of MSP1 supplemented with an N-terminal His-tag, a TEV protease recognition site, and a linker **(Figure 1.7A)**. The addition of the His-tag has several practical benefits, including the use of Ni-NTA affinity chromatography for purification and detection of MSP1D1 by Western blot. When required, the TEV protease can be used to selectively cleave the His-tag while leaving the MSP1D1 protein intact[60].

Nanodisc self-assembly occurs when the detergent is removed from the reconstitution mixture containing MSP, lipids, and the target membrane protein **(Figure 1.7B)**. Careful optimization of the lipid to MSP and target to MSP molar ratios is important for the successful

incorporation of the target membrane protein into the nanodiscs[61]. The lipid composition can also be modified to better mimic the native membrane environment of the protein of interest. Commonly used lipids include POPC, POPE, *E. coli* polar lipid extracts and soybean polar lipid extracts. Together, these features make nanodiscs a useful tool for membrane protein structural studies, including single particle cryo-EM, where the absence of detergent micelles helps improves particle contrast and signal in vitreous ice[62]. In this study, nanodiscs were used to reconstitute ABCG5/G8 in a lipid bilayer in order to capture the transporter in a native like environment for high resolution cryo-EM structural studies.

Figure 1.7. Schematic representation of the MSP1D1 construct and nanodisc assembly.
(A) Domain architecture of the MSP1D1 construct, showing the N-terminal His-tag (blue) and TEV protease recognition site (orange) preceding the main MSP sequence (green). **(B)** Illustration of a nanodisc reconstituted with a membrane protein (orange), in which two copies of the MSP (green) encircle a phospholipid bilayer (gray) in a belt like arrangement. Figure created with BioRender.com.

1.7. Single Particle Cryo-Electron Microscopy

Single particle cryo-electron microscopy (cryo-EM) has become a powerful method for high resolution structure determination of biological macromolecules, in particular membrane proteins. In a typical cryo-EM experiment, a purified sample is applied to a holey grid, blotted and rapidly plunge frozen in liquid ethane to trap molecules in vitreous ice[63]. The vitrified grid is imaged in a transmission electron microscope using direct electron detectors, producing two-

dimensional projection images of particles in various orientations. These images are then computationally aligned and averaged to reconstruct a 3D density map[64].

Recent advances in direct electron detector technology, image processing algorithms and microscope stability have led cryo-EM to routinely achieve near atomic resolution in the "resolution revolution"[65]. "The combination of cryo-EM with nanodiscs has been especially valuable, allowing membrane proteins to be imaged in a native like lipid environment without the drawbacks of detergent[62]. In this thesis, single particle cryo-EM was used to determine the structure of ABCG5/G8 reconstituted in nanodisc, four combinations of MSP (MSP1D1 and MSP1E3D1) and lipid (POPC and E. coli polar lipid extract).

1.8. Nanobodies as Structural and Therapeutic Tools

Considerable progress has been made in the fields of structural biology and antibody based therapies, offering potential avenues for the development of new treatments. Antibodies have long been a cornerstone in both diagnostic and therapeutic applications due to their ability to bind specifically and with high affinity to target molecules[66]. In the context of ABCG5/G8, the cryo-EM structure of the transporter in complex with Fab fragments from two monoclonal antibodies (mAbs) demonstrated that antibody binding can modulate the ATPase activity of ABCG5/G8 **(Figure 1.8)**. However, because of the limited ability of antibodies to cross the plasma membrane and reach intracellular epitopes, they cannot be employed as therapeutic agents[53]. While mAbs have shown efficacy in treating various conditions, their large size presents several challenges. This includes difficulties in targeting intracellular components and molecular cavities, constraints in the methods of drug delivery, and elevated costs of production[67].

In recent years, nanobodies have emerged as particularly powerful tools to overcome many of these limitations. Nanobodies are single domain variable fragments derived from heavy chain

only antibodies (HCAbs) naturally produced by camelids, including camels, llamas, and alpacas **(Figure 1.9)**[68] .

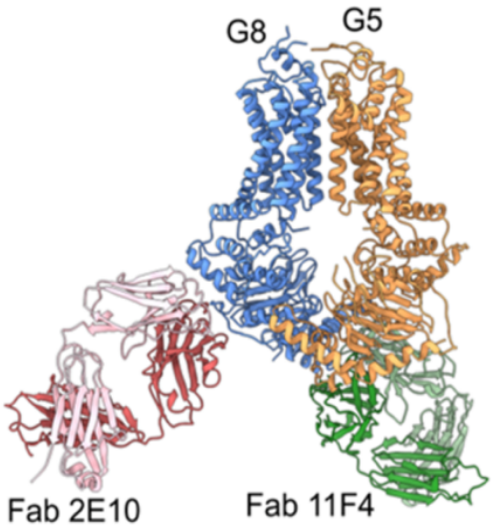

Figure 1.8. Cryo-EM structure of ABCG5/G8 in complex with modulating antibodies.
Cartoon representation of the ABCG5/G8 heterodimer (ABCG5 in yellow, ABCG8 in blue) bound by the Fab fragments of two modulating monoclonal antibodies, Fab 2E10 (pink/red) and Fab 11F4 (green). The two Fabs bind at distinct sites on the nucleotide binding domains and have opposing effects on the ATPase activity of ABCG5/G8. Figure adapted from Zhang et al. (2021).

Unlike conventional antibodies, which are composed of both heavy and light chains, HCAbs lack light chains and contain a single variable domain on each heavy chain, referred to as VHH or nanobody, which alone is sufficient for antigen recognition. Their small size, high stability, solubility and specificity make them promising tools for both structural biology and therapeutic applications[69].

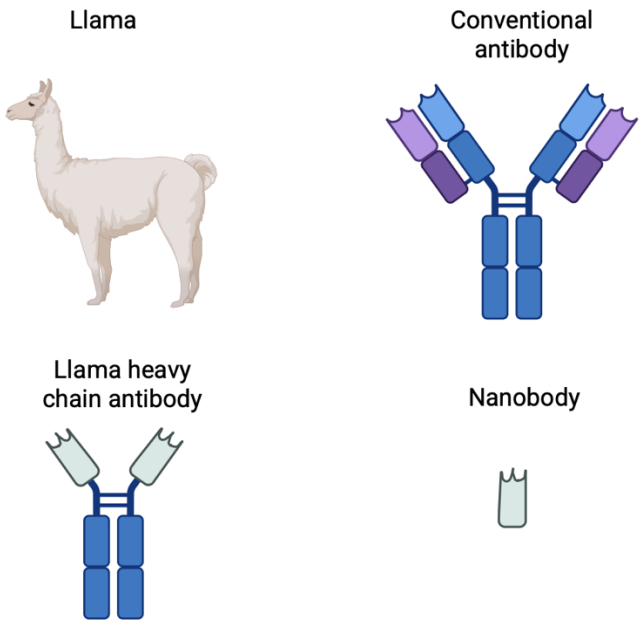

Figure 1.9. Comparison of conventional antibodies and camelid derived nanobodies.
Schematic representation of a conventional antibody (top right), composed of two heavy chains (blue) and two light chains (purple), each containing variable and constant domains. In contrast, camelids such as llamas (top left) produce heavy-chain only antibodies (HCAbs, bottom left) that lack light chains and possess a single variable domain on each heavy chain. The isolated variable domain of HCAbs, called nanobody or VHH (bottom right, green). Figure created with BioRender.com.

The small size of nanobodies is one of their most significant advantages. It allows access to epitopes that are typically inaccessible to larger conventional antibodies, including conformation specific binding sites within membrane proteins and protein complexes[68]. Furthermore, nanobodies can be produced recombinantly in bacterial and yeast expression systems, which makes it easy to produce them on a large scale and engineer them for downstream applications[70]. These properties make nanobodies particularly attractive for the development of biologic based drugs targeting emerging infectious diseases and chronic diseases, as well as powerful tools for high resolution structural studies of dynamic and challenging targets such as membrane proteins[71].

To date, nanobodies have been developed against several ABC transporters, including ABCG2 where novel nanobodies were generated and three inhibitory clones were identified through functional screening; these nanobodies were shown to bind and modulate ABCG2 transporter activity[72]. However, no nanobodies against ABCG5/G8 have been reported. The unique properties of nanobodies could be utilized to develop new strategies for the precise regulation of ABCG5/G8 function, representing a significant advancement in the management of diseases such as sitosterolemia where ABCG5/G8 dysfunction is a key contributor. Also, the use of nanobodies in this context may improve our understanding of the molecular mechanisms behind cholesterol transport and metabolism, with further implications for the treatment of cardiovascular and metabolic diseases. In this thesis, a yeast surface display nanobody library[73] was screened to identify nanobodies binding to ABCG5/G8, with the aim of producing reagents that could serve as structural tools for future cryo-EM studies as well as potential therapeutic candidates targeting this transporter. To address this, I have carried out the following three specific aims to achieve this project.

2. Methodological Background

Determining the structure of a membrane protein such as ABCG5/G8 involves a series of interdependent methods, each addressing a specific challenge: producing the protein in a properly folded state, extracting it from the membrane without denaturation, purifying it to homogeneity, returning it to a lipid environment, confirming its stability, and ultimately imaging it at high resolution. This chapter outlines the physical principles underlying each method and the rationale for their selection in this project, following the experimental workflow from expression through structural analysis. The complementary nanobody-generation workflow is

presented at the conclusion, as it provides tools for both structural studies and potential therapeutic applications.

2.1. Expression and Purification of Membrane Proteins

Membrane proteins are responsible for numerous essential cellular functions and represent a major class of therapeutic drug targets. However, they remain among the most challenging proteins to study structurally. Because endogenous levels are too low for structural analysis, these proteins are typically produced recombinantly using a heterologous expression system[74]. Their hydrophobic transmembrane regions, conformational flexibility, and instability outside the lipid bilayer present significant challenges for expression, folding, solubilization, and purification[75]. Efficient production relies on the selection of a suitable host and the optimization of conditions for expression and subsequent processing.

The selection of an expression host is primarily determined by the requirements of the target protein. Bacterial systems, such as *Escherichia coli*, are cost-effective and yield high levels of protein; however, they lack the post-translational modification pathways necessary for eukaryotic membrane proteins, which can result in improperly folded or modified proteins[76]. Yeast represents an effective compromise by combining eukaryotic folding and processing capabilities, such as N-glycosylation, with lower costs and greater scalability compared to mammalian or insect-cell systems[77]. This system has been successfully used for the production of functional ABC transporters[78]. This is particularly important for ABCG5/G8, because N-glycosylation is required for proper maturation and trafficking of the heterodimer[29].

ABCG5/G8 was expressed in the methylotrophic yeast *Pichia pastoris*, with the transporter genes integrated into the genome under the control of the alcohol oxidase 1 (PAOX1) promoter. The PAOX1 promoter is repressed during growth on glucose or glycerol and is strongly induced

by periodic methanol supplementation to sustain expression[79]. Expression conditions influence both protein yield and the proportion of correctly folded protein. Consequently, induction temperature and duration must be optimized for each target protein. Rapid expression at higher temperatures may increase total yield but can overwhelm cellular folding and membrane-insertion machinery, resulting in aggregation or misfolding, whereas slower expression at lower temperatures can favour proper folding. For ABCG5/G8, expression conditions were chosen to prioritize the production of correctly folded, membrane-integrated protein over maximal total yield.

Membrane proteins are localized within the lipid bilayer via hydrophobic transmembrane regions and are therefore insoluble in aqueous buffer without intervention. Extracting ABCG5/G8 in its native conformation requires disrupting the membrane with detergent. Detergents, amphipathic molecules with both hydrophilic and hydrophobic domains, form micelles above their critical micelle concentration. These micelles encapsulate the protein's transmembrane surfaces and replace membrane lipids, maintaining protein solubility in solution[80]. Selecting an appropriate detergent involves balancing extraction efficiency with protein stability. Smaller, more aggressive detergents effectively solubilize membranes but may remove stabilizing lipids and destabilize proteins. In contrast, milder detergents typically preserve native structure and activity, although they may be less efficient at extraction. Consequently, detergent screening is often necessary to identify conditions that maintain both solubility and stability of the target protein[81].

Once solubilized, ABCG5/G8 was purified using immobilized-metal affinity chromatography (IMAC). The protein carries a polyhistidine tag that binds to Ni^{2+} ions on the column, while most untagged proteins are washed away. The bound protein is then eluted with a

high concentration of imidazole, which competes with the histidine tag for binding. Lower concentrations of imidazole are included during loading and washing to reduce weak, non-specific interactions and improve sample purity. Affinity purification enriches ABCG5/G8 based on its His-tag, but it does not show whether the protein is correctly folded or aggregated. A second purification step based on size is therefore needed to isolate the properly assembled heterodimer.

The affinity-purified ABCG5/G8 sample was further purified by size-exclusion chromatography (SEC), which separates molecules based on size. Larger species elute earlier because they cannot enter the pores of the column beads, while smaller species take a longer path and elute later. SEC removes aggregates and other contaminants and also provides a measure of sample quality. A single, symmetric peak indicates a homogeneous sample, whereas early peaks or shoulders suggest aggregation or heterogeneity. For this reason, SEC was used as the final quality-control step before structural studies.

SDS-PAGE was used to assess the composition and purity of the ABCG5/G8 sample. For ABCG5/G8, the gel confirms the presence of both subunits and shows whether major contaminants are present. Because the proteins are denatured during SDS-PAGE, this method does not show whether the heterodimer is correctly folded or assembled, which is instead assessed by SEC.

2.2. Nanodisc Reconstitution

Although detergents maintain membrane protein solubility, they do not fully replicate the lipid bilayer and may destabilize proteins over time. To better mimic the native membrane environment, the purified ABCG5/G8 transporter was reconstituted into nanodiscs. Nanodiscs are small patches of lipid bilayer surrounded by two membrane scaffold proteins (MSPs), which

shield the hydrophobic edges and maintain particle solubility[57]. This allows ABCG5/G8 to remain in a defined lipid bilayer, facilitating structural studies.

Membrane scaffold proteins (MSPs) are available in various lengths, with scaffold size directly influencing nanodisc diameter. Smaller variants, such as MSP1D1, form discs approximately 10 nm in diameter, whereas larger variants, including MSP1E3D1 and MSP2N2, generate bigger lipid patches. The optimal scaffold depends on the size of the membrane protein, since a disc that is too small can crowd the protein, while a very large disc may introduce extra flexibility. In this work, smaller MSP1D1 and larger MSP1E3D1 was used for cryo-EM preparation. Two lipid environments were tested: POPC, a single defined phospholipid that forms a stable, fluid bilayer, and E. coli polar lipid extract, a more complex mixture containing several lipid species, including anionic lipids. Comparing a single defined lipid with a native-like mixture makes it possible to test whether the transporter's stability or structure depends on the lipid environment.

The membrane scaffold protein was expressed in *Escherichia coli* using a T7/lac expression system, in which IPTG induces high-level transcription. For nanodisc assembly, purified ABCG5/G8, membrane scaffold protein, and phospholipids were combined in detergent at a defined molar ratio. Detergent was gradually removed using adsorbent beads, enabling the lipids and MSP to self-assemble around the transporter and form discrete nanodiscs[61]. Nanodisc size is determined by the MSP variant, while lipid and protein ratios are optimized to yield stable particles containing ABCG5/G8. Nanodiscs offer several advantages for studying ABCG5/G8. They provide a defined and adjustable lipid bilayer with a known composition, avoid the uncertainty associated with detergent micelles, and can improve protein stability while maintaining a particle suitable for cryo-EM[54].

2.3. Thermal stability by nano-differential scanning fluorimetry

Nano-differential scanning fluorimetry (nano-DSF) was used to assess whether nanodisc reconstitution improved ABCG5/G8 stability. The method monitors the intrinsic fluorescence of tryptophan residues as the protein is heated. In the folded state, tryptophans are usually buried in a more hydrophobic environment, but unfolding exposes them to the more polar solvent and shifts their fluorescence. The change in the 350/330 nm fluorescence ratio is used to determine the melting temperature (Tm), which provides a measure of protein thermal stability[82].

Nano-DSF utilizes the protein's intrinsic tryptophan fluorescence, eliminating the need for external dyes. This approach is advantageous for membrane proteins, as detergents and lipids may interfere with dye-based assays. A higher melting temperature reflects increased thermal stability; therefore, comparing detergent-solubilized and nanodisc-reconstituted ABCG5/G8 can determine whether the lipid bilayer enhances protein stability.

2.4. Single particle Cryo-EM

The structure of ABCG5/G8 was determined using single-particle cryo-electron microscopy (cryo-EM). The purified protein was applied to a grid, blotted into a thin layer, and rapidly frozen in liquid ethane to form vitreous ice, preserving the particles and preventing the formation of damaging ice crystals. Frozen particles were imaged using an electron microscope, resulting in numerous two-dimensional particle images. These images were subsequently aligned, classified, and computationally combined in cryoSPARC to generate a three-dimensional density map[83]. Advances in detector technology and image processing now allow cryo-EM to routinely reach near-atomic resolution[65].

A sample that looks good in solution may still perform poorly on a cryo-EM grid because problems can arise during vitrification. After blotting, particles become confined within a thin layer of water and rapidly encounter the air–water interface[84]. This interface can partially denature particles or cause them to adopt preferred orientations, reducing the quality of the final reconstruction.

Therefore, cryo-EM grids require screening and optimization even when the protein is stable and monodisperse in solution. The process of grid preparation can introduce additional challenges, especially at the air–water interface. Nanodiscs can provide further protection for membrane proteins by encapsulating them within a lipid bilayer and scaffold, instead of relying mainly on detergent micelles.

2.5. Nanobody Library Screening

To identify binders against ABCG5/G8, a synthetic nanobody library was screened using yeast-surface display. Nanobodies, or VHHs, are small (~15 kDa) single-domain antibody fragments derived from camelid heavy-chain antibodies. Their small and rigid structure makes them useful for cryo-EM because they can bind specific regions or conformations of a target and may help stabilize particular states.

In yeast-surface display, a large synthetic nanobody library is displayed on the surface of Saccharomyces cerevisiae, with each cell carrying a different nanobody[73]. The cells are incubated with purified ABCG5/G8, and binders are selected while non-binders are removed. Repeating this process enriches the strongest binders, which are then identified by sequencing.

3. Thesis Objectives

ABCG5/G8 plays an essential role in maintaining sterol homeostasis by mediating the transport of cholesterol and plant sterols. Dysfunction of this heterodimeric transporter is associated with sitosterolemia and an increased risk of cardiovascular disease. Although major progress has been made in the structural characterization of ABCG5/G8, several important questions remain unresolved. Available structures have been determined either in detergent micelles or in restrictive lipid environments, which may not fully replicate the native membrane environment of the transporter and could limit the ability to capture functionally relevant conformational states. Additionally, because the transport cycle of ABC transporters is intrinsically dynamic, it may be challenging to capture conformational changes associated with substrate binding and ATP hydrolysis under typical conditions. To address these limitations, this thesis aimed to establish a nanodisc based system for structural studies of ABCG5/G8 and to identify ABCG5/G8 specific nanobodies that could serve as molecular tools for future biochemical and cryo-EM studies of the transporter.

2.1 Expression, Purification, and Nanodisc Reconstitution of ABCG5/G8.

To express and purify human ABCG5/G8 from *Pichia pastoris* and to systematically optimize its reconstitution into nanodiscs of different sizes of membrane scaffold proteins (MSP1D1 and MSP1E3D1) and lipid compositions (POPC and E. coli polar lipid extract) to identify conditions resulting in homogenous and stable samples for downstream structural studies.

2.2 Cryo-EM Structural Studies of ABCG5/G8.

To determine the cryo-EM structure of nanodisc reconstituted ABCG5/G8 in different sample conditions, including the apo state, in the presence of cholesterol, and in the presence of cholesterol and the non-hydrolysable ATP analog AMP-PNP, with the goal of gaining structural insights into

the transporter in a native like lipid bilayer environment and establishing conditions that can be used for further structural studies.

2.3 Identification of ABCG5/G8 specific nanobodies.

To screen a yeast surface display nanobody library for nanobodies that bind specifically to ABCG5/G8, offering novel tools that could be used as structural tools in future cryo-EM studies, while also providing candidates that could be further investigated as potential modulators or therapeutic agents. Together, these objectives aimed to improve the structural study of ABCG5/G8 in a lipid bilayer environment and to establish new tools for future mechanistic and therapeutic investigations of this sterol transporter.

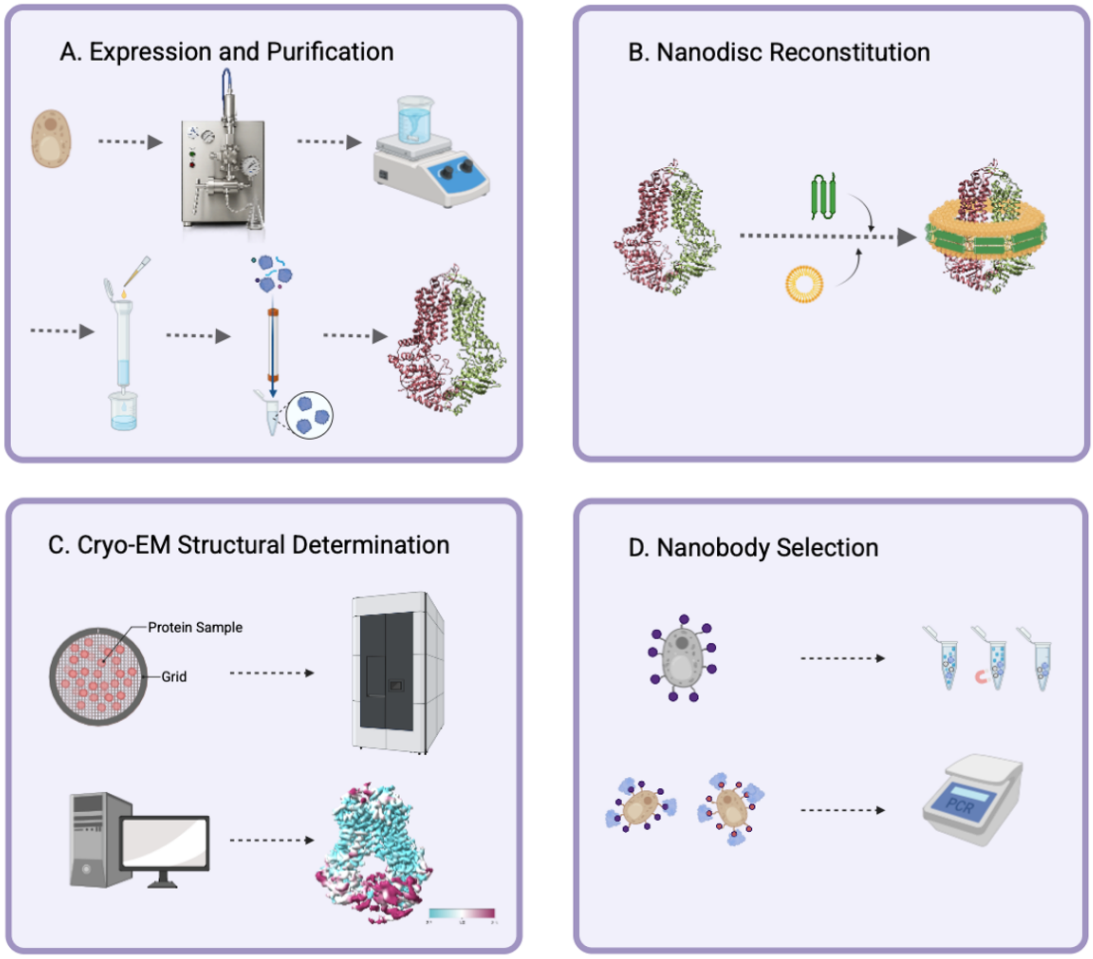

Figure 3.1. **Overview of the experimental workflow in this thesis for the structural and functional study of ABCG5/G8.**

(A) Wild type ABCG5/G8 was expressed in *Pichia pastoris*, solubilized from membranes with DDM/CHS, and purified by Ni-NTA affinity chromatography followed by size exclusion chromatography. **(B)** Purified ABCG5/G8 was reconstituted into nanodiscs by detergent removal with Bio Beads. **(C)** Nanodisc reconstituted ABCG5/G8 was vitrified onto Quantifoil grids and imaged by single particle cryo-EM on a Titan Krios G4 microscope, yielding a 3D reconstruction of ABCG5/G8 at 3.15 Å resolution. **(D)** In parallel, a yeast surface display nanobody library was subjected to four rounds of magnetic bead-based selection against detergent purified ABCG5/G8 at progressively decreasing antigen concentrations, yielding five unique ABCG5/G8 binding nanobodies following sequencing and CDR analysis. Figure created with BioRender.com.

4. Materials

4.1. General Buffers and Media

Reagent / Buffer	Composition
Kanamycin (1000×)	50 mg/mL kanamycin sulfate in H_2O
LB medium (per liter)	10 g peptone, 5 g yeast extract, 5 g NaCl in H_2O, sterilize by autoclaving
TB medium (per liter)	12 g tryptone, 24 g yeast extract, 4 mL glycerol, 17 mM KH_2PO_4, 72 mM K_2HPO_4 in H_2O, sterilize by autoclaving
10× YNB stock (per liter)	100 g ammonium sulfate, 34 g yeast nitrogen base in H_2O, filter sterilize
1000× biotin stock	40 mg biotin in 100 mL H_2O (NaOH added to dissolve)
MGY medium (per liter)	1% (v/v) glycerol, 1× YNB, 1× biotin in H_2O, sterilize by autoclaving; induction with 0.5% (v/v) methanol; pH maintained at 5–6 with 10% (v/v) ammonium hydroxide
–Trp + Glucose medium (per liter)	3.8 g yeast synthetic drop-out medium supplement (without tryptophan), 6.7 g yeast nitrogen base, 10 mL Pen-Strep (10,000 units/mL stock), 20 g glucose, adjusted to pH 6.0, sterilized by autoclaving (antibiotic added after autoclaving)
–Trp + Galactose medium (per liter)	3.8 g yeast synthetic drop-out medium supplement (without tryptophan), 6.7 g yeast nitrogen base, 10 mL Pen-Strep (10,000 units/mL stock), 20 g galactose, adjusted to pH 6.0, sterilized by autoclaving (antibiotic added after autoclaving)
–Trp + Glucose agar plates	–Trp + Glucose medium supplemented with 2% (w/v) agar

4.1.1 Buffers for ABCG5/G8 Purification

Reagent / Buffer	Composition
Cell lysis buffer (with protease inhibitors)	0.33 M sucrose, 0.3M Tris-HCl pH 7.5, 0.1 M ε-aminocaproic acid, 1 mM EDTA, 1 mM EGTA, 1 mM PMSF, 1 μg/mL leupeptin, 1 μg/mL pepstatin A, 20 mM β-mercaptoethanol in H_2O

Reagent / Buffer	Composition
Membrane resuspension buffer	50 mM Tris-HCl pH 8.0, 150 mM NaCl, 10% (v/v) glycerol, 1 mM PMSF, 1 µg/mL leupeptin, 1 µg/mL pepstatin A, 20 mM β-mercaptoethanol in H_2O
Solubilization buffer	50 mM Tris-HCl pH 8.0, 150 mM NaCl, 0.5% sodium cholate, 1% DDM, 0.1% CHS, 1 mM PMSF, 1 µg/mL leupeptin, 1 µg/mL pepstatin A, 20 mM β-mercaptoethanol in H_2O
Ni-NTA equilibration / wash 1 buffer	50 mM Tris-HCl pH 8.0, 150 mM NaCl, 0.25% sodium cholate, 5% (v/v) glycerol, 0.3% DDM, 0.03% CHS, 25 mM imidazole in H_2O
Ni-NTA wash 2 buffer	50 mM Tris-HCl pH 8.0, 150 mM NaCl, 0.25% sodium cholate, 5% (v/v) glycerol, 0.3% DDM, 0.03% CHS, 50 mM imidazole in H_2O
Ni-NTA elution buffer	50 mM Tris-HCl pH 8.0, 150 mM NaCl, 0.25% sodium cholate, 5% (v/v) glycerol, 0.3% DDM, 0.03% CHS, 200 mM imidazole in H_2O
SEC buffer (ABCG5/G8)	50 mM Tris-HCl pH 7.5, 150 mM NaCl, 0.03% DDM, 0.003% CHS, 0.05% sodium cholate in H_2O

4.1.2 Buffers for MSP1D1 / MSP1E3D1 Purification

Reagent / Buffer	Composition
Lysis buffer	50 mM Tris-HCl pH 8.0, 300 mM NaCl, 1 mM PMSF, 1 µg/mL leupeptin, 1 µg/mL pepstatin A in H_2O
Buffer A (Wash 1)	40 mM Tris-HCl pH 8.0, 300 mM NaCl, 1% Triton X-100 in H_2O
Buffer B (Wash 2)	40 mM Tris-HCl pH 8.0, 300 mM NaCl, 50 mM sodium cholate, 20 mM imidazole in H_2O
Buffer C (Wash 3)	40 mM Tris-HCl pH 8.0, 300 mM NaCl, 50 mM imidazole in H_2O
Buffer D (Elution)	40 mM Tris-HCl pH 8.0, 300 mM NaCl, 500 mM imidazole in H_2O
Dialysis buffer	20 mM Tris-HCl pH 7.5, 150 mM NaCl

4.1.3 Buffers for Nanodisc Reconstitution

Reagent / Buffer	Composition
Lipid solubilization buffer	20 mM Tris-HCl pH 7.5, 150 mM NaCl, 200 mM sodium cholate in H_2O
Nanodisc SEC buffer	20 mM Tris-HCl pH 7.5, 150 mM NaCl in H_2O

4.1.4 Buffers and Solutions for SDS-PAGE

Reagent / Buffer	Composition
Coomassie staining solution	20% (v/v) methanol, 10% (v/v) acetic acid, 0.25% Coomassie R-250 (w/v) in H_2O
Destaining solution	30% (v/v) ethanol, 10% (v/v) acetic acid in H_2O

4.1.5 Buffers for Yeast Surface Display Nanobody Screening

Reagent / Buffer	Composition
Equilibration / wash buffer (EW buffer)	50 mM Tris-HCl pH 7.5, 150 mM NaCl, 100 mM imidazole, 0.03% DDM, 0.003% CHS in H_2O
Elution buffer	50 mM Tris-HCl pH 7.5, 150 mM NaCl, 250 mM imidazole, 0.03% DDM, 0.003% CHS in H_2O

5. Methods

5.1. Protein Biochemical Methods

5.1.1 MSP Expression

MSP1D1 and MSPE3D1 are expressed using the pET expression system (Novagen) with the BL21-Gold (DE3) *E. coli* strain (Stratagene) as a host. To generate the starter culture, a single colony grown on fresh plates was used to inoculate kanamycin containing LB (50 mg/L) broth, after which the culture was incubated overnight at 37°C with shaking at 250 rpm. The starter culture was used to inoculate 1 L Terrific Broth (TB), which was further incubated at 37°C with shaking at 250 rpm. Cell growth was monitored by measuring absorbance at 600 nm (OD600), and once the culture reached an OD600 of 2, protein expression was induced by adding IPTG to a final concentration of 1 mM. Induction was carried out for 3 hours at 37°C. Cells were then collected by centrifugation at 4000 rpm for 40 minutes, and the final cell pellets were stored at -80°C until further use.

5.1.2 MSP Purification

The pellet of 1L cells was resuspended in 90 mL lysis buffer. Sonication method was used to disrupt the cells, and this was done using alternating 30 second on and off cycles for 3 minutes. Triton X-100 was then added from a 10% stock solution to make a 1% final concentration, and after solubilization of the mixture was done for 30 minutes at 4°C, the solution was then loaded onto 5 mL Ni-NTA affinity column. The column was successively washed using three different buffers, each added in an amount equivalent to 10 column volumes (CVs) Buffer A-C, elution was done with Buffer D. Protein concentration was measured, and the protein sample was diluted to 2

mg/mL using dialysis buffer and left for overnight dialysis. The dialyzed protein was further concentrated using a spin concentrator to a final concentration of 9 mg/mL and kept at -80°C.

5.1.3 Recombinant ABCG5/G8 Expression in *Pichia Pastoris*

The expression of the ABCG5/G8 gene constructs in *Pichia pastoris* was performed using the method outlined in Lee et al. (2016). Initially, yeast cells were cultured on MD plates by spreading 50 μL of the glycerol stock culture through a sterile spatula over the entire plate surface, after which they were incubated at 30 °C for 48 hours. The plates were then kept at 4 °C and could be stored for up to a month.

The starter cultures consisted of six 50 mL tubes with 10 mL of MGY medium that were inoculated with the cells using a sterile loop. These starter cultures were then incubated for 24 hours at 30 °C under agitation at 250 rpm. Each starter was then used to inoculate 1 L of MGY medium in a 2.8 L Fernbach flask, resulting in a 6 L total culture volume. The cultures were grown at 30 °C under agitation at 250 rpm in an Innova 43 shaker (New Brunswick). The pH of the culture was continuously maintained in a pH range between 5 and 6 by adding 10% NH4OH when necessary. When the pH was stabilized, the cultures were allowed to grow further for another 12 hours before induction.

Protein expression was induced by the addition of methanol 5 mL (0.5% v/v) every 12 hours over a total induction period of 36–48 hours. Cells were harvested by centrifugation at 4,200 rpm for 20 minutes at 4 °C. The pellets obtained were suspended in lysis buffer according to a 1:1 ratio of buffer volume to cell weight in grams, and the suspension was kept at −80 °C. The usual amount of cells obtained was 40 ± 5 g/L.

5.1.4 Cell Lysis and Membrane Preparation

Frozen cell pellets were thawed and lysed with a C3 Emulsiflex homogenizer (Avestin) in lysis buffer supplemented with protease inhibitors. The suspension was passed through the homogenizer three times at a pressure of 25,000 to 30,000 psi. The lysate was clarified by centrifugation at 4,000 × g for 15 minutes and then at 15,000 × g for 30 minutes, both at 4 °C, to remove unbroken cells and debris.

To pellet the microsomal membranes, the supernatant was ultracentrifuged at 42,000 rpm for two hours at 4 °C using a Beckman 45Ti rotor. Protease inhibitor containing microsomal membrane buffer was used to resuspend the resulting membrane pellets using a Dounce homogenizer, and they were then kept at -80 °C until needed.

5.1.5 Solubilization

Thawed membranes were mixed with an equal volume of solubilization buffer containing 2% DDM and 0.2% CHS, and the mixture was gently stirred for 1 hour at 4 °C. After solubilization, insoluble membrane material was removed by ultracentrifugation at 30,000 rpm using a Beckman 45Ti rotor for 30 minutes at 4 °C. The resulting clarified supernatant was used protein purification.

5.1.6 Protein Purification by Affinity Chromatography

Affinity chromatography was carried out using packed 10 ml nickel-nitrilotriacetic acid (Ni-NTA, Qiagen) resin at 4 °C. Column washed with milli-Q H2O and equilibrated with wash buffer A. The supernatant was incubated with Ni-NTA resin for a maximum of 12h. The column was washed sequentially with 10 column volumes of wash buffer 1 containing 25 mM imidazole followed by 10 column volumes of wash buffer 2 containing 50 mM imidazole to remove non-specifically

bound proteins. Target proteins were eluted with elution buffer containing 200 mM imidazole and collected in one third column volume fractions. Peak fractions were identified by Bradford assay, pooled, and concentrated to a final volume of 0.5–1 mL using a 100 kDa molecular weight cut off centrifugal concentrator, spun at 3,000 × g in 5-minute intervals at 4 °C.

5.1.7 Size-Exclusion Chromatography (SEC)

Size exclusion chromatography was performed on an ÄKTA FPLC system at 4 °C. Protein was detected on elution profiles by absorbance at 280 nm. All buffers were freshly filtered and degassed before use. After each run, the columns were stored in either 20% ethanol or Milli-Q water.

Protein purification was performed on Superdex 200 Increase 10/300 GL column. The sample volume of 0.1–0.5 mL was injected using a sample loop of 1 mL, and runs were performed at a flow rate of 0.5 mL/min while keeping the column pressure below 3 MPa. During the run 0.3 mL fractions were collected. The protein fractions were then evaluated by SDS-PAGE analysis.

5.1.8 Protein Concentration

The protein samples were concentrated using Vivaspin centrifugal filter units with molecular weight cut offs ranging from 10 kDa to 100 kDa, depending on the target protein size and all filtration units were equilibrated with the appropriate buffer before use.

5.1.9 Determination of Protein Concentration

Protein concentration was determined using a bicinchoninic acid (BCA) protein assay kit, following the manufacturer's instructions. Bovine serum albumin (BSA) was used as a protein standard to generate a standard curve over a concentration range of 0–1000 μg/mL. Samples and

standards were prepared in duplicate and incubated with the BCA working reagent at 37 °C for 30 minutes. A microplate reader was used to measure absorbance at 562 nm, and the standard curve was plotted to determine protein concentrations. To calibrate, we also use SDS-PAGE to confirm the protein concentrations.

5.1.10 SDS-PAGE Gel Electrophoresis

Protein samples were resolved on 10% polyacrylamide gels of either 1.0 mm or 1.5 mm thickness, using SDS running buffer at a constant voltage of 140 V for 45 minutes at room temperature. Following electrophoresis, gels were stained with Coomassie staining solution for 30 minutes with gentle agitation, then destained overnight. Gels were subsequently washed with Milli-Q water and scanned for comparison of apparent molecular weights.

5.2. Nanodisc Reconstitution

5.2.1 Lipid Preparation

POPC and E. coli polar lipid were dissolved in chloroform at a concentration of 25 mg/ml, transferred to a glass vial, and dried under a gentle nitrogen stream in a fume hood to form a thin, evenly distributed lipid film. Residual solvent was removed by placing the vials in a desiccator under medium vacuum. The lipid film was subsequently resuspended in lipid solubilization buffer to achieve a final lipid concentration of 100 mM. Complete solubilization was ensured by vortexing, heating in hot water, and sonicating in an ultrasonic bath until no visible lipid remained on the vial walls.

5.2.2 Nanodisc Reconstitution

Membrane protein reconstitution into nanodiscs relies on the self-assembly of membrane scaffold proteins (MSPs) around a phospholipid bilayer, such as POPC. To reconstitute the membrane protein into nanodiscs, lipid, MSP, and membrane protein were combined at the following molar ratios, for all ABCG5/G8 to MSP is 1:5

- MSP1D1 / POPC 1:50
- MSP1D1 / *E. coli* lipid 1:20
- MSP1E3D1 / POPC 1:130
- MSP1E3D1 / *E. coli* lipid 1:55

The final mixture was transferred to a 1 ml Eppendorf tube and incubated at 4 °C for 1 hour, a temperature close the phase transition of both POPC and E. coli lipids. To start reconstitution, the detergents sodium cholate (Na-cholate) and n-dodecyl-β-D-maltoside (DDM) were removed by gradually adding activated SM-2 Bio-Beads. Initially, 0.2 g of Bio-Beads were added, and the mixture was incubated for 2 hours on a rotating wheel at 4 °C. This step was repeated by adding successively 0.3 g and 0.5 g of Bio-Beads, for a total amount of 1 g. After the final addition, the reconstitution mixture was incubated overnight on a rotating wheel at 4 °C.

5.2.3 Thermostability analysis

The thermostability of ABCG5/G8 was assessed using differential scanning fluorimetry and dynamic light scattering on an Uncle instrument (NRC-Ottawa). This was used to compare the thermal stability and aggregation behavior of detergent solubilized ABCG5/G8 and ABCG5/G8 reconstituted into MSP1D1/POPC nanodiscs. Prior to analysis, all samples were centrifuged at

14,000 rpm for 10 min at 4°C. Detergent solubilized ABCG5/G8 was analyzed at 2 mg/mL in 50 mM Tris-HCl pH 7.5, 150 mM NaCl, 0.03% DDM, 0.003% CHS, and 0.05% sodium cholate. Nanodisc reconstituted ABCG5/G8 was analyzed at 2.2 mg/mL in 20 mM Tris-HCl pH 7.5 and 150 mM NaCl.

Samples were loaded in triplicate and heated while monitoring changes in intrinsic protein fluorescence to determine the melting temperature (T_m). In parallel, dynamic light scattering was used to monitor aggregation temperatures (T_{agg}). and hydrodynamic diameter at 25°C. The resulting thermal transition profiles were analyzed using Uncle Analysis Software (version 6.01, Unchained Labs) to determine T_m, T_{agg}, and particle size distribution and replicate values are reported as the mean ± standard deviation (n = 3).

5.3. Nanobody Selection and Characterization

5.3.1 Nanobody library Recovery and Expansion

One cryovial of the yeast nanobody library (NbLib) from Kruse lab[73] was thawed at 30 °C for 5–10 min and added to 750 mL Yglc4.5–Trp medium. The culture was incubated overnight at 30 °C with shaking 230 rpm. The next day 250 mL of the culture were transferred to 750 mL of fresh Yglc4.5–Trp medium. This procedure was repeated twice, to reach a total culture volume of 3 L. The culture was incubated at 30 °C and 230 rpm for 48 h. After expansion the OD600 of the culture was measured and diluted if necessary to keep the readings within the linear range of detection (1 OD600 = 1.5 × 10^7 yeast cells/mL). Cells were harvested by centrifugation at 3,500 × g for 5 minutes at 4 °C and the supernatant was discarded. The yeast pellet was resuspended in Yglc4.5–Trp medium supplemented with 10% DMSO to a final cell density of 1×10^{10} cells/mL. 1 mL aliquot were dispensed into 2 mL cryovials and stored at −80 °C.

5.3.2 Nanobody library Induction

A total of 1×10^{10} cells of the expanded NbLib were thawed at 30 °C for 5–10 minutes and transferred into 10 mL of Yglc4.5–Trp medium. The culture was incubated at 30 °C with shaking at 220 rpm overnight. The next day, cells were harvested by centrifugation at 3,500 × g for 5 minutes at 25 °C and the supernatant was discarded. The yeast pellet was resuspended in 5 mL of –Trp+Gal medium and then transferred into 145 mL of –Trp+Gal medium to a total volume of 150 mL. The culture was incubated at 25 °C with shaking at 220 rpm for 48 hours to allow surface expression of the nanobody library.

The OD_{600} of the culture was measured after induction and diluted with –Trp+Gal medium as necessary to ensure accurate readings in the linear detection range (1 $OD_{600} \approx 1.5 \times 10^7$ cells/mL). Cells were harvested by centrifugation at 3,500 × g for 5 min at 4 °C and the supernatant was discarded. Yeast pellet was resuspended in EW buffer to a final cell density of 1.1 × 10 10 cells/mL and kept on ice.

5.3.3 Nanobody Selection and preclearing

His Mag Sepharose Ni beads were transferred to a microcentrifuge tube and collected using a magnetic separation rack. The storage solution was discarded, and the beads were washed once with 1 mL of sterile ddH_2O and twice with 1 mL of EW buffer, collecting beads magnetically and discarding the supernatant after each wash. The yeast suspension was then incubated with the equilibrated beads on a rotary mixer for 1.5 hours at 4 °C to deplete non specific binders. Beads were collected by magnetic separation rack, and the pre-cleared supernatant was transferred to a

new centrifuge tube. Cells were harvested by centrifugation at 3,500 × g for 5 minutes at 4 °C and resuspended in the EW Buffer.

For the ABCG5/G8 experiments, 1 μM final concentration of ABCG5/G8 was added to the yeast suspension and rotated for 1 h at 4 °C. His Mag Sepharose Ni beads (25 μL settled beads per 2.5 × 10^9 cells) were equilibrated as described in the pre-clearing step and added to the yeast-protein suspension. The mixture was rotated for 1 h at 4 °C to capture His-tagged protein bound yeast cells. The supernatant was discarded and the beads were collected magnetically. Beads were washed 3 times with 1 mL EW buffer, collecting beads magnetically and discarding supernatant between washes.

Cells attached to the beads were eluted by incubating the beads with 1 mL of Elution buffer for 5 min at 4 °C. The eluate (E1) was collected by magnetic separation and transferred to a new microcentrifuge tube. This elution step was repeated twice to obtain fractions E2 and E3. All eluate fractions were pooled and centrifuged at 3,500 × g for 3 minutes at 25 °C to pellet yeast cells and the supernatant was discarded. The yeast pellet was then resuspended in 1 mL of –Trp+Glc medium, repelleted at 3,500 × g for 3 minutes at 25 °C and finally resuspended in 3 mL of –Trp+Glc medium. The culture was incubated at 30 °C with shaking at 220 rpm for 24 hours to recover.

After recovery, the culture was harvested by centrifugation at 3,500 × g for 3 minutes at 25 °C and the supernatant was discarded. The yeast pellet was resuspended in 3 mL of –Trp+Gal medium and incubated at 25 °C with shaking at 220 rpm for 48 hours to induce surface expression of the nanobody library.

The selection procedure for round 2 was carried out as described for Round 1, except that ABCG5/G8 at a lower concentration of 250 nM was used. The yeast pellet was then recovered after elution and resuspended in 3 mL of –Trp+Glc medium and incubated at 30 °C shaking at 220 rpm for 24 hours.

Round 3 was performed by repeating the induction and selection procedures described for Round 2, using ABCG5/G8 at a lower concentration of 75 nM. Round 4 was subsequently performed following the same procedure at a further reduced concentration of 15 nM.

5.3.4 Isolation of Single Yeast Colonies and Sequencing

After the final round of selection, yeast cells were plated onto –Trp+Glc agar plates (150 µL per plate) on two plates and incubated upside down at 30 °C for 2–3 days. Individual colonies were selected and streaked on fresh -Trp+Glc agar plates for duplication and stored at 4 °C.

For sequencing, colony PCR was performed using heat-popped yeast cells. Briefly, a small amount of yeast from each colony was resuspended in 50 µL of sterile water in an Eppendorf tube. A 15 µL aliquot of the suspension was transferred to a PCR tube and heat lysed at 99 °C for 5 min and then cooled to 4 °C. The PCR reaction was performed in a total volume of 20 µL using 2 µL of heat-popped yeast lysate as template, with the following cycling conditions: initial denaturation at 98 °C for 30 s, followed by 35 cycles of 98 °C for 10 s, 60 °C for 10 s, and 72 °C for 30 s with a final extension at 72 °C for 10 min. PCR products were separated on 1.5% agarose gel and bands of expected size were excised and quantified. DNA was sent out for Sanger sequencing using the pYDS649 forward primer (5’-GACTTCGACGCTGCTGCTTTG-3’). The resulting sequences

were analyzed and aligned in Benchling and colonies expressing nanobodies were identified and selected based on the presence and diversity of complementarity-determining regions (CDRs).

5.4. Single Particle Cryo-Electron Microscopy

5.4.1 Sample Preparation

Table 3. Summary of ABCG5/G8 nanodisc sample conditions tested for cryo-EM grid preparation
Concentration of ABCG5/G8 nanodisc samples were adjusted 0.5 to 1 mg/ml. All samples were solved on SEC buffer with Tris and NaCl. Different cholesterol concentrations were tested across conditions, as ethanol used for cholesterol solubilization was found to adversely affect overall grid quality at higher concentrations.

Sample	Lipid	Conditions
MSP1E3D1/*E. coli* APO*	*E. coli* polar lipid	—
MSP1E3D1/*E. coli* + Cholesterol*	*E. coli* polar lipid	0.01 mM cholesterol
MSP1E3D1/*E. coli* + Cholesterol + AMP-PNP*	*E. coli* polar lipid	0.01 mM cholesterol, 5 mM AMP-PNP, 5 mM $MgCl_2$
MSP1E3D1/POPC APO*	POPC	—
MSP1E3D1/POPC + Cholesterol*	POPC	0.033 mM cholesterol
MSP1E3D1/POPC + Cholesterol + AMP-PNP*	POPC	0.02 mM cholesterol, 5 mM AMP-PNP, 5 mM $MgCl_2$
MSP1D1/POPC + Cholesterol	POPC	0.033 mM cholesterol
MSP1D1/POPC + Cholesterol + AMP-PNP	POPC	0.02 mM cholesterol, 5 mM AMP-PNP, 5 mM $MgCl_2$
MSP1D1/*E. coli* APO	*E. coli* polar lipid	—
MSP1D1/*E. coli* + Cholesterol	*E. coli* polar lipid	0.01 mM cholesterol
MSP1D1/*E. coli* + Cholesterol + AMP-PNP	*E. coli* polar lipid	0.01 mM cholesterol, 5 mM AMP-PNP, 5 mM $MgCl_2$

**Conditions selected for final cryo-EM data collection.*

5.4.2 Cryo-EM Grid Preparation

Freshly purified ABCG5/G8 was reconstituted in nanodiscs in SEC buffer and incubated with either cholesterol or cholesterol and AMP-PNP prior to grid preparation (see Table 1). Quantifoil R1.2/1.3 copper grids (300 mesh) were washed with chloroform and glow discharged using a PELCO easiGlow at 15 mA for 45 sec. Four microliters of each sample were applied onto the grids and vitrified at 4 °C under 100% humidity using a Vitrobot Mark IV device, with 597 filter papers, a blot force of 20, and a blotting time of 4 seconds prior to plunge freezing in liquid ethane.

5.4.3 Data Acquisition

Cryo-EM data were collected on a Titan Krios G4 transmission electron microscope (MPI-Frankfurt) operating at 300 kV, equipped with a FEI Falcon 4 direct electron detector. Data were collected at a nominal magnification of 215,000× with pixel size of 0.573 Å. Movies were collected with 50 frames per movie, a total electron dose of 50 $e^{-}/Å^{2}$, and an exposure time of 2.3 s per movie. The defocus range was set to −1 to −2 μm. A total of 9,634, 7,541, and 12,110 micrographs were collected for the APO, cholesterol incubated, and cholesterol and AMP-PNP incubated datasets, respectively.

Before automated data collection, gain reference and magnetization settings were calibrated. Data collection was carried out using EPU software in electron counting mode. Automated procedures for alignment including eucentric height adjustment and image shift calibration were used.

DSF measurement and analysis was performed by Dr. Jamshid Tanha and Sophie Wen (NRC-Ottawa). Data acquisition and processing were performed by Haoran Fu (MPI-Frankfurt).

6. Results

6.1. MSP1D1 Expression and Purification Optimization

Bacterial growth conditions can influence the expression of MSP1D1, effecting both protein yield and quality. To increase MSP1D1 yield and quality, different established protocols were tested for growth and purification conditions. Initially, induction for 6 hours at 30 °C in LB medium was tested, which resulted in a low protein amount **(Figure 6.1A)**. A second protocol using overnight induction at 18 °C in LB medium resulted in a relatively higher yield **(Figure 6.1B)**. Based on these results, a third protocol using 3-hour induction at 37 °C in TB medium was followed, which produced the highest quantity of MSP1D1 and was therefore used for all future preparations **(Figure 6.1C)**.

Effect of growth medium on cell density and protein yield was tested by comparison of Luria-Bertani (LB) broth and Terrific Broth (TB). The wet cell pellet from 2L of culture grown in TB medium weighed ~40g, while the wet pellet from LB media weighed ~20g. These results demonstrate that the nutritionally rich TB medium gives significantly higher cell densities and protein yields **(Figure 6.1C)**.

After Ni-NTA affinity chromatography fractions were dialyzed overnight against dialysis buffer. All optimized conditions such as TB medium, 3-hour induction at 37 °C and dialysis based purification had been used to give a final amount of 40 mg of MSP1D1 as confirmed by SDS-PAGE as a dominant band at approximately 25 kDa (**Figure 6.1C)**. The same optimized protocol was then used for MSP1E3D1, resulting in a final amount of 60 mg of protein, which was analyzed

by SDS-PAGE as a major band at approximately 35 kDa, consistent with the molecular weight of MSP1E3D1 **(Figure 6.1D)**.

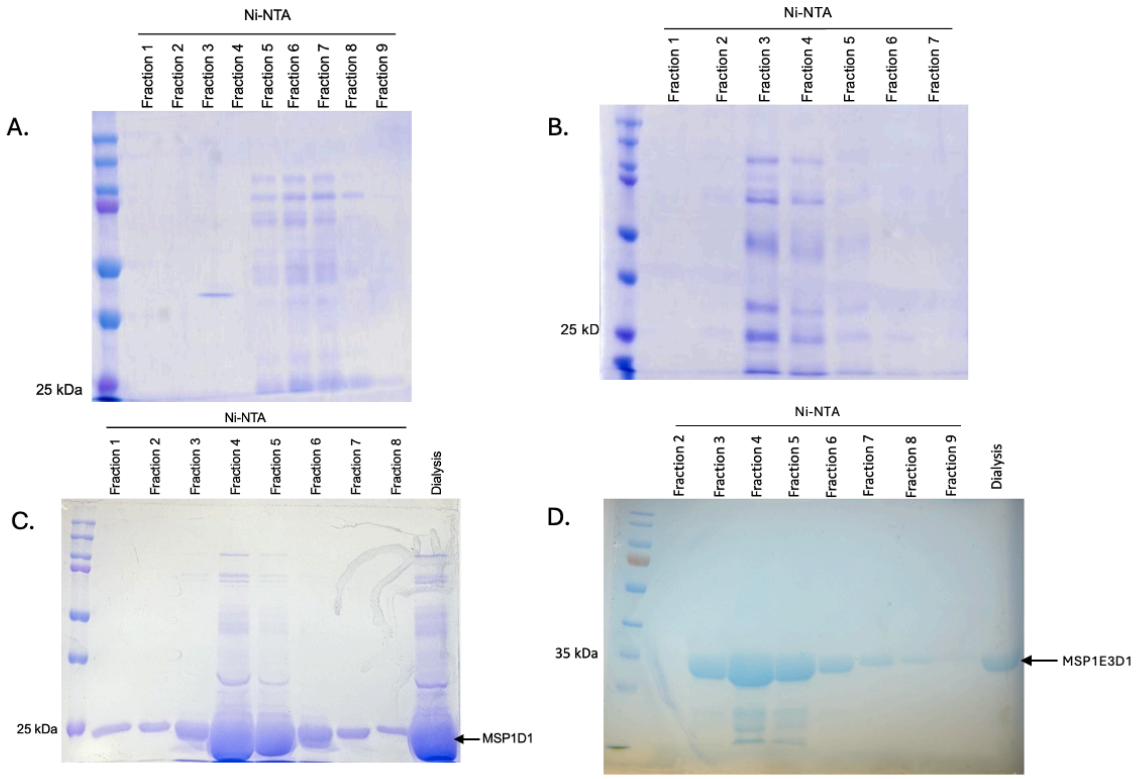

Figure 6.1. SDS-PAGE analysis of MSP1D1 and MSP1E3D1 expression and purification under different conditions.
Ni-NTA fractions were analyzed by SDS-PAGE and visualized by Coomassie Blue staining. The position of the molecular mass marker is indicated on the left of each gel. (**A**) MSP1D1 expressed in LB medium and induced with 1 mM IPTG for 6 h at 30 °C. Fractions 1–9 (1 mL each) were collected after Ni-NTA affinity chromatography. (**B**) MSP1D1 expressed in LB medium and induced overnight with 1 mM IPTG at 18 °C. Fractions 1–7 (1.6 mL each) were collected after Ni-NTA affinity chromatography. (**C**) MSP1D1 expressed in TB medium and induced with 1 mM IPTG for 3 h at 37 °C. Fractions 3–6 from Ni-NTA affinity chromatography were dialyzed overnight against dialysis buffer; the final dialysis sample is shown in the last lane. (**D**) MSP1E3D1 expressed in TB medium and induced with 1 mM IPTG for 3 h at 37 °C using the same optimized protocol as in (C). Fractions 3–6 from Ni-NTA affinity chromatography were dialyzed overnight; the final dialysis sample is shown in the last lane. The expected molecular weights of MSP1D1 (~25 kDa) and MSP1E3D1 (~35 kDa) are indicated by arrows.

6.2. Membrane Protein Purification

Wild-type ABCG5/G8 was recombinantly expressed in *Pichia pastoris* for single particle cryo-EM and nanobody library screening. Proteins were solubilized from cell membranes using 1% (w/v) DDM and 0.1% (w/v) CHS and purified using a C-terminal His_6-tag. Purity was checked by

SDS-PAGE. The purified protein was either reconstituted into MSP nanodiscs for structural analysis by cryo-EM or directly used for nanobody library screening.

6.3. ABCG5/G8 Purification

ABCG5/G8 purification followed the protocol in Chapter 2. Following solubilization, unwanted proteins were removed during the Ni-NTA purification step. After elution with 200 mM imidazole, samples were concentrated and subjected to size exclusion chromatography using a Superdex 200 column.

The SEC chromatogram displays a major peak with a retention volume of approximately 10.5 to 11 mL, consistent with the expected size of the ABCG5/G8 heterodimer (~150 kDa), indicating a monodisperse and homogeneous preparation **(Figure 6.2A)**. Occasionally, a small shoulder was observed on the leading edge of the main peak, which may suggest the presence of a minor proportion of aggregates. In these cases, only the major peak fractions were collected to maintain sample quality for downstream applications.

SDS-PAGE analysis of the pooled and concentrated SEC fractions showed two distinct bands at approximately 75 kDa, corresponding to the ABCG5 and ABCG8 **(Figure 6.2B)**.

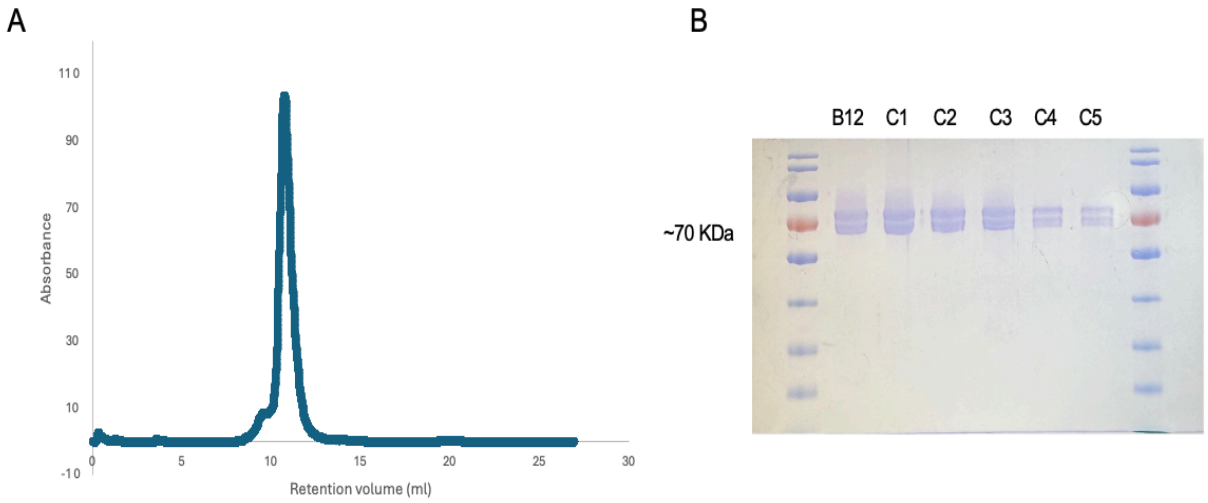

Figure 6.2. SEC and SDS-PAGE analysis of purified ABCG5/G8.
(A) SEC chromatogram of purified ABCG5/G8 was performed on a Superdex 200 column, showing a peak at ~10.5 mL retention volume consistent with the ABCG5/G8 heterodimer. **(B)** SDS-PAGE analysis of SEC fractions (B12–C5) showing two bands at ~75 kDa corresponding to the ABCG5/G8.

The thermal stability of purified ABCG5/G8 heterodimer was measured by differential scanning fluorimetry (DSF) using the Uncle instrument on detergent solubilized and MSP1D1/POPC nanodisc reconstituted samples **(Table 2)**. The detergent solubilized sample showed primary and secondary melting temperature of Tm1 = 59.87 ± 0.40 °C and Tm2 = 77.54 ± 1.64 °C and aggregation temperature (Tagg) of 42.90 ± 0.24 °C. All three parameters have been increased when reconstituted into MSP1D1/POPC nanodiscs with Tm1 of 61.65 ± 1.59 °C, Tm2 of 81.61 ± 2.23 °C and Tagg of 45.40 ± 2.60 °C. These results suggest that ABCG5/G8 has a higher thermal stability in nanodiscs, possibly because of the lipid bilayer providing a more native like environment that better maintains the structural integrity of the transporter.

Table 4. Thermostability parameters for detergent solubilized and nanodisc reconstituted ABCG5/G8
The melting temperature (T_m) reflects the temperature induced protein unfolding, while the aggregation temperature (T_{agg}) indicates the onset of protein aggregation as determined by Uncle. Nanodisc reconstitution increases both T_m and T_{agg}, suggesting enhanced thermal stability compared to the detergent sample. Values are expressed as mean ± SD.

Sample	**T_m1 M±SD** (°C)	**T_m2 M±SD** (°C)	**T_{agg} M±SD** (°C)
ABCG5/G8 in detergent	59.87 ± 0.40	77.54 ± 1.64	42.90 ± 0.24
ABCG5/G8 Nanodisc	61.65 ± 1.59	81.61 ± 2.23	45.40 ± 2.60

6.4. Nanodisc Reconstitution Optimization

In order to identify the optimal conditions for reconstitution of ABCG5/G8 into nanodiscs for cryo-EM structural studies, four reconstitution conditions were tested, combining two MSP variants (MSP1D1 and MSP1E3D1) with two lipid compositions (POPC and E. coli polar lipid extract) at molar ratios of 1:50 for MSP1D1:POPC, 1:20 for MSP1D1:E. coli, 1:130 for MSP1E3D1:POPC, and 1:55 for MSP1E3D1:E. coli and for all ABCG5/G8:MSP is 1:5. All four conditions were subjected to SEC and SDS-PAGE after reconstitution, and selected conditions were then further evaluated by cryo-EM grid preparation and screening.

SEC analysis of the MSP1D1/POPC reconstitution revealed two peaks at approximately 15 mL and 16 mL retention volume, corresponding to ABCG5/G8 containing nanodiscs and empty nanodiscs respectively, however an aggregation shoulder was observed beginning at ~9 mL **(Figure 6.3)**. SDS-PAGE confirmed the presence of both ABCG5/G8 subunits at ~75 kDa and MSP1D1 at ~25 kDa in the nanodisc fractions. **(Figure 6.3)**. Despite the successful reconstitution confirmed by SDS-PAGE, cryo-EM grid screening of the MSP1D1/POPC condition revealed an insufficient number of particles and poor overall grid quality. The presence of ethanol, used for cholesterol solubilization, which seemed to have a negative effect on particle distribution across the grid prevented further data collection **(Figure 6.3)**.

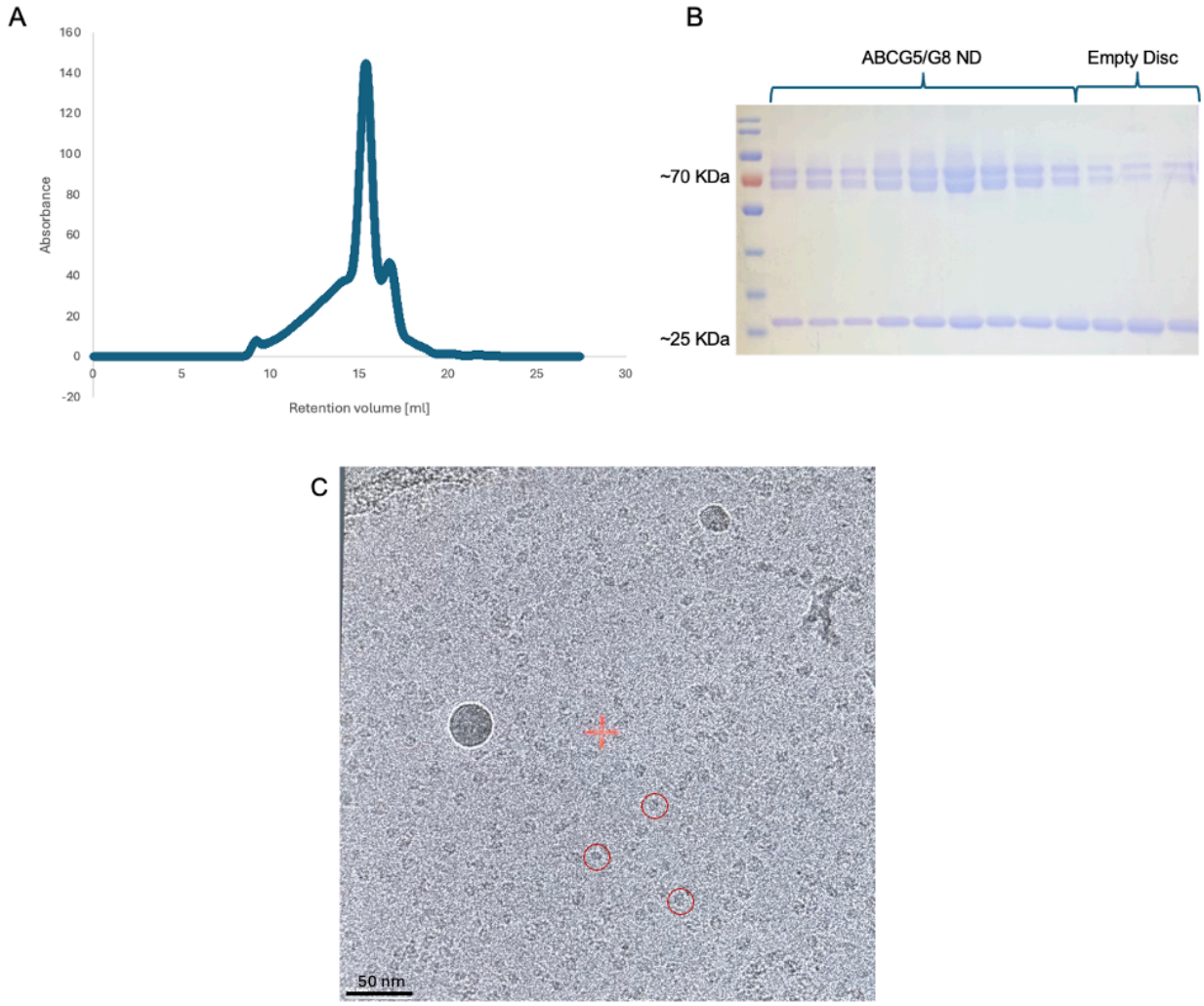

Figure 6.3. SEC and SDS-PAGE analysis of ABCG5/G8 reconstituted into MSP1D1/POPC nanodiscs. **(A)** SEC chromatogram of ABCG5/G8 reconstituted into MSP1D1/POPC nanodiscs, was perfomed on a Superose 6 column, showing a major peak at ~15 mL corresponding to ABCG5/G8 nanodiscs, a second peak at ~16 mL corresponding to empty nanodiscs, and a minor shoulder at ~9 mL possible aggregates. **(B)** SDS-PAGE analysis of SEC fractions showing bands at ~75 kDa corresponding to ABCG5 and ABCG8 and ~25 kDa corresponding to MSP1D1 in the ABCG5/G8 nanodisc fractions. **(C)** Micrograph of ABCG5/G8 reconstituted into MSP1D1/POPC nanodiscs incubated with AMP-PNP and cholesterol. Based on the poor grid quality during screening, MSP1D1/POPC was not used for further for cryo-EM data collection. Particles circled in red. Scalebar, 50 nm.

The MSP1D1/E. coli polar lipid reconstitution displayed a large peak at ~15 mL retention volume corresponding to the nanodiscs with ABCG5/G8 and two smaller peaks at ~16-17 mL corresponding to empty nanodiscs, and an aggregation shoulder at ~9 mL, indicating

heterogeneous mixture of nanodisc populations of different sizes **(Figure 6.4A-B)**. Based on the poor grid screening results obtained with MSP1D1/POPC, cryo-EM grids prepared from the MSP1D1/*E. coli* condition were not screened further.

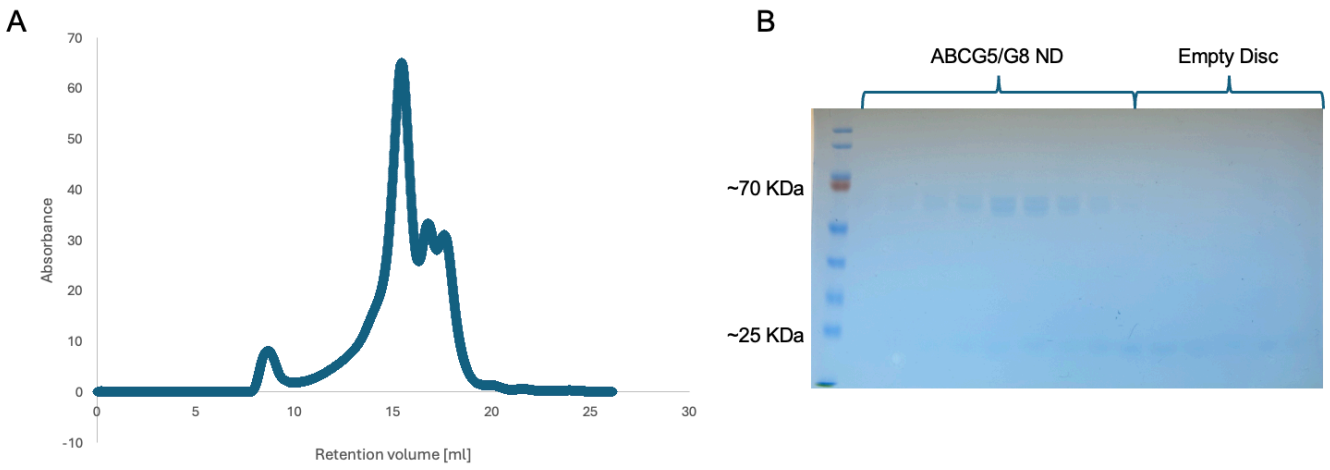

Figure 6.4. **SEC and SDS-PAGE analysis of ABCG5/G8 reconstituted into MSP1D1/E. coli lipid nanodiscs.**
(A) SEC chromatogram of ABCG5/G8 reconstituted into MSP1D1/E. coli lipid nanodiscs, was performed on a Superose 6 column, showing a major peak at ~15 mL corresponding to ABCG5/G8 containing nanodiscs, two peaks at ~16–17 mL corresponding to empty nanodiscs, and a minor shoulder at ~9 mL indicative of aggregates. **(B)** SDS-PAGE analysis of SEC fractions showing bands at ~75 kDa corresponding to ABCG5 and ABCG8 and ~25 kDa corresponding to MSP1D1 in the ABCG5/G8 nanodisc fractions. Empty nanodisc fractions show only the MSP1D1 band at ~25 kDa.

Reconstitution of ABCG5/G8 with MSP1E3D1 and E. coli polar lipids resulted in an SEC profile showing two major peaks at ~15-16 mL retention volume corresponding to nanodiscs containing ABCG5/G8 and empty nanodiscs respectively, with a minor peak at ~9 mL, corresponding a small amount of aggregates **(Figure 6.5A)**. SDS-PAGE showed the expected bands of ~75 kDa for ABCG5/G8 and ~35kDa for MSP1E3D1 **(Figure 6.5B)**. Cryo-EM grid screening showed visually suitable grids **(Figure 6.5C)**, but initial 2D classification after Cryo-EM data collection, resulted

in low resolution class averages with poorly defined features, potentially indicating conformational flexibility of the protein in the larger MSP1E3D1 nanodisc environment of E. coli lipids.

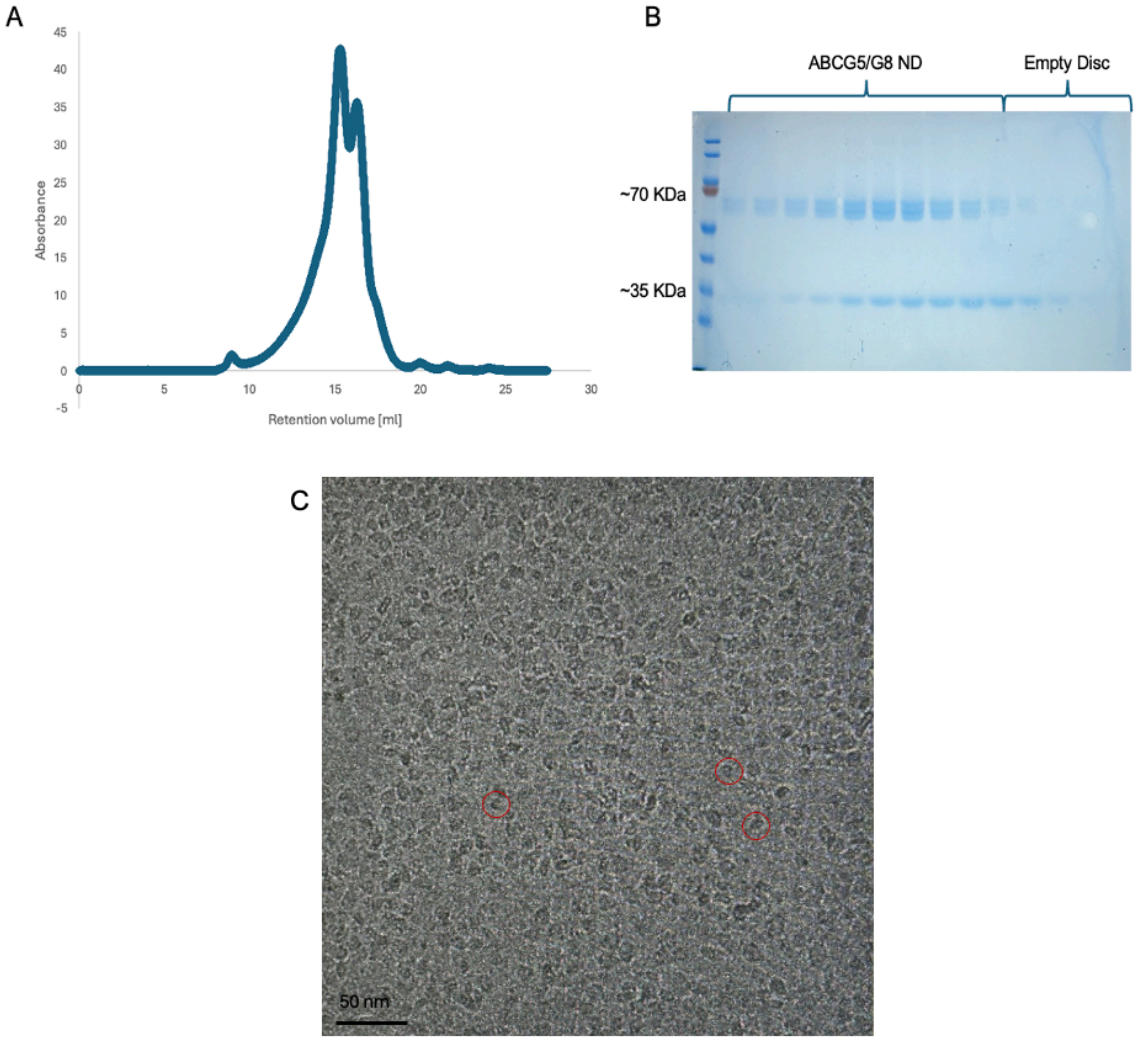

Figure 6.5. SEC and SDS-PAGE analysis of ABCG5/G8 reconstituted into MSP1E3D1/*E. coli* lipid nanodiscs.
(A) SEC chromatogram of ABCG5/G8 reconstituted into MSP1E3D1/*E. coli* lipid nanodiscs, recorded on a Superose 6 column, showing two peaks at ~15 mL and ~16 mL corresponding to ABCG5/G8 containing nanodiscs and empty nanodiscs respectively, and a minor shoulder at ~9 mL indicating some aggregates. **(B)** SDS-PAGE analysis of SEC fractions showing bands at ~75 kDa corresponding to ABCG5 and ABCG8 subunits and ~35 kDa corresponding to MSP1E3D1 in the ABCG5/G8 nanodisc fractions. Empty nanodisc fractions show only the MSP1E3D1 band at ~35 kDa. **(C)** Cryo-EM micrograph of ABCG5/G8 reconstituted into MSP1E3D1/*E. coli* lipid nanodiscs, the micrograph shows a grid square with evenly distributed particles across the vitrified ice, indicating successful grid preparation. Despite good particle distribution, 2D classification yielded low resolution class averages with poorly defined structural features, and this condition was therefore not used for further for data processing. Particles circled in red. Scale bar, 50 nm.

In contrast, reconstitution of ABCG5/G8 with MSP1E3D1 and POPC resulted in the most favourable SEC profile with two well defined peaks at ~15–16 mL corresponding to ABCG5/G8 containing nanodiscs and empty nanodiscs, respectively, with minimal aggregation **(Figure 6.6A)**. Analysis by SDS-PAGE showed two bands corresponding to ABCG5 and ABCG8 around 75 kDa, and a band corresponding to MSP1E3D1 around 35 kDa in the ABCG5/G8 nanodisc fractions. In the empty nanodisc control, only the MSP1E3D1 band was observed **(Figure 6.6B)**. After grid preparation for cryo-EM, grids with good particle distribution and ice quality were obtained **(Figure 6.6C)**. Based on these results, MSP1E3D1/POPC was chosen as the best reconstitution condition for all subsequent cryo-EM data collection, processing and model building.

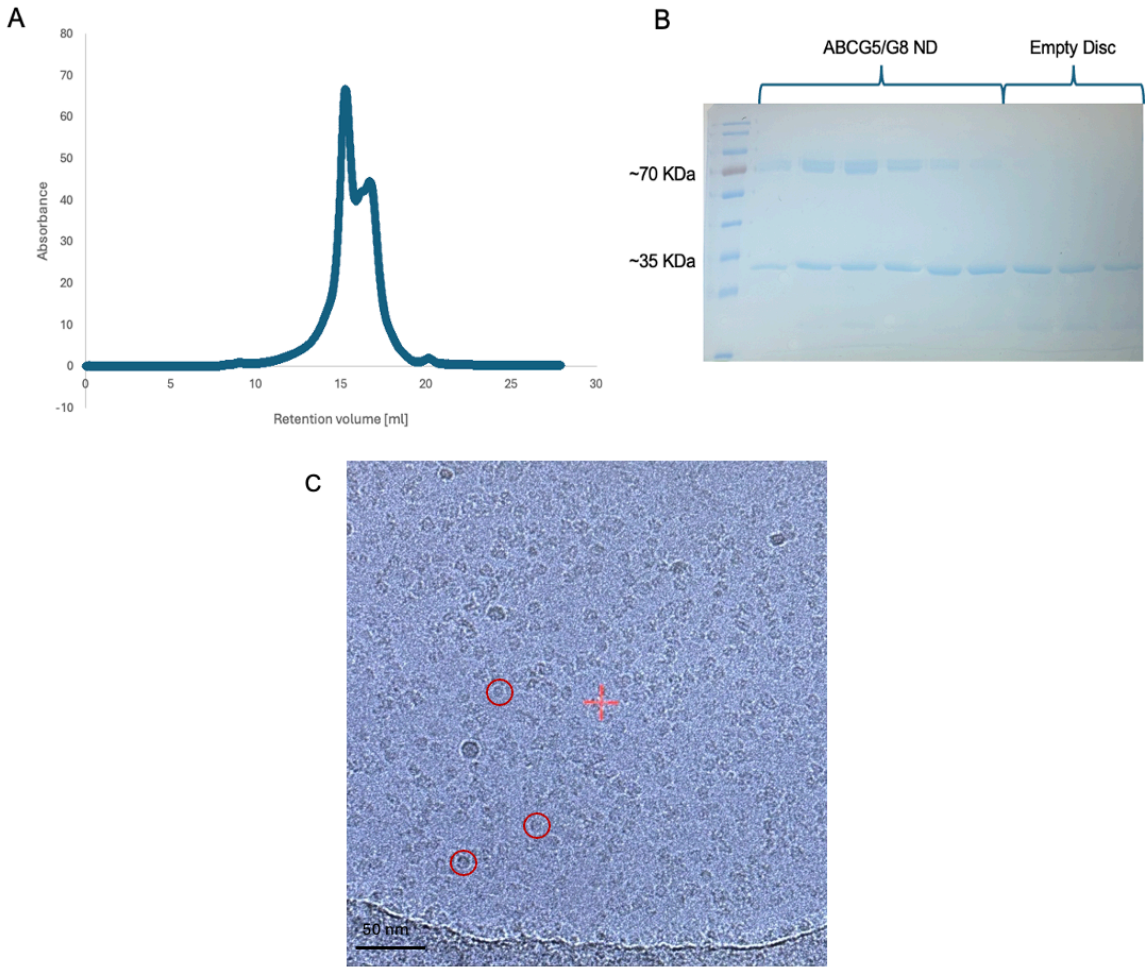

Figure 6.6. SEC and SDS-PAGE analysis of ABCG5/G8 reconstituted into MSP1E3D1/POPC nanodiscs. **(A)** SEC chromatogram of ABCG5/G8 reconstituted into MSP1E3D1/POPC nanodiscs, recorded on a Superose 6 column, showing two peaks at ~15 mL and ~16 mL corresponding to ABCG5/G8 containing nanodiscs and empty nanodiscs respectively, with minimal aggregation. **(B)** SDS-PAGE analysis of SEC fractions showing bands at ~75 kDa corresponding to ABCG5 and ABCG8 and ~35 kDa corresponding to MSP1E3D1 in the ABCG5/G8 nanodisc fractions. Empty nanodisc fractions show only the MSP1E3D1 band at ~35 kDa. **(C)** Cryo-EM micrograph of ABCG5/G8 reconstituted into MSP1E3D1/POPC nanodiscs. The micrograph shows a representative grid square with well distributed particles in vitreous ice of suitable thickness, indicating good grid preparation. Particles are clearly visible and evenly distributed across the grid surface with no significant aggregation. Particles circled in red. Scale bar, 50 nm. This condition was selected for full cryo-EM data collection and high resolution model building based on the good particle distribution and ice quality observed during grid screening.

6.5. Cryo-EM maps of nanodisc reconstituted ABCG5/G8

To obtain structural information, six sample conditions were selected for single particle cryo-electron microscopy (cryo-EM) analysis of the ABCG5/G8 heterodimer reconstituted in MSP1E3D1 nanodiscs. Samples were prepared in either E. coli polar lipid or POPC nanodiscs and included apo conditions, cholesterol incubated conditions, and cholesterol with the non-hydrolyzable ATP analogue AMP-PNP. Although all six conditions were collected, only the POPC nanodisc samples produced 2D classes of sufficient quality to proceed with high resolution reconstruction and model building.

A summary of all samples and their conditions is given in Table 1 of Chapter 2. Samples were vitrified onto Quantifoil R1.2/1.3 copper grids, giving uniformly distributed particles suitable for cryo-EM data collection. Three datasets were collected and processed for the APO, cholesterol-incubated, and cholesterol and AMP-PNP incubated conditions. Data processing and refinement were carried out by Haoran Fu. An exemplary processing workflow for the ABCG5/G8 MSP1E3D1 APO dataset is shown in **Figure 6.7**. Briefly, following motion correction and CTF estimation, automated particle picking and initial 2D classification were performed. Selected 2D class averages showing well defined structural features were used to train the TOPAZ particle picking model, yielding a total of 806,175 initial particles for the dataset. The selected 2D classes were subsequently used for ab initio reconstruction in cryoSPARC, generating three initial 3D models, of which the best resolved class was selected and subjected to heterogeneous refinement.

The highest quality class from heterogeneous refinement was then carried forward for 3D refinement and polishing steps, resulting in the final high resolution reconstruction.

All three maps had local resolution estimates between 2.7 and 3.3 Å, with the core transmembrane area showing the best resolution and the nucleotide binding domain showing the lowest **(Figure 6.8A)**. According to the FSC 0.143 criterion, CryoSPARC data processing achieved final reconstructions at overall resolutions of 3.15 Å, 3.26 Å, and 3.58 Å for the APO, chl, and chl+AMP-PNP conditions, respectively **(Figure 6.8B)**. In the cholesterol or chl+AMP-PNP conditions, no cholesterol density was found, and there were no significant conformational changes across the three conditions. These results suggest that the ligand concentrations were not sufficient to saturate the binding site or the incubation condition and time were not enough to induce a stable conformational change. The conditions used for ligand incubation will possibly need further optimization in order to capture specific structural states of ABCG5/G8.

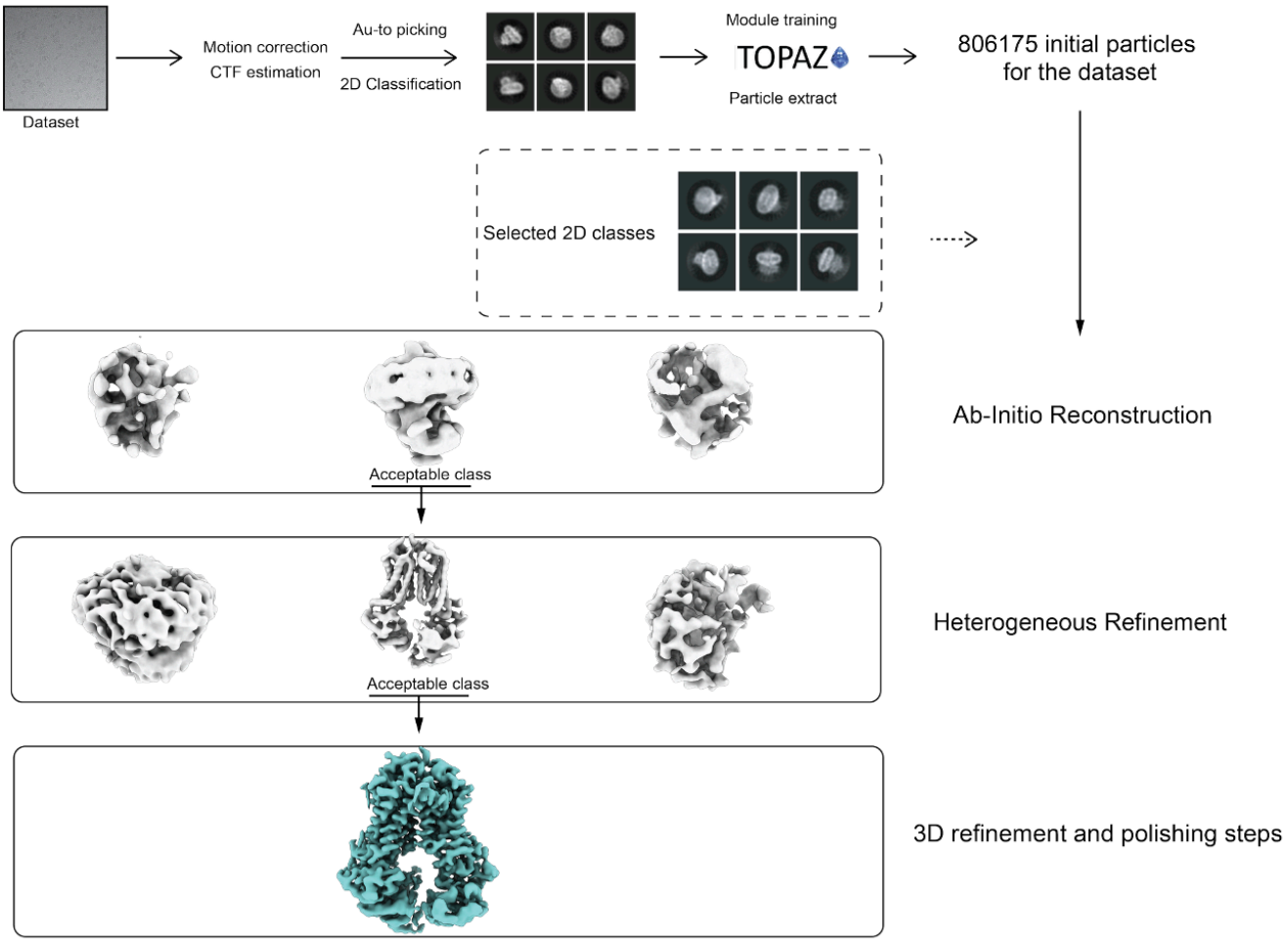

Figure 6.7. Cryo-EM data processing workflow for ABCG5/G8 in nanodiscs.
Cryo-EM micrograph and 2D class averages of nanodisc reconstituted ABCG5/G8. Particle picking was performed with TOPAZ giving an improved 2D classes with clear structural features. 3D classification and refinement steps were used to obtain a homogenous subset of particles and to improve the quality of the map. The final cryo-EM density map at 3.15 Å resolution shows the overall architecture of ABCG5/G8 in a native like lipid bilayer environment.

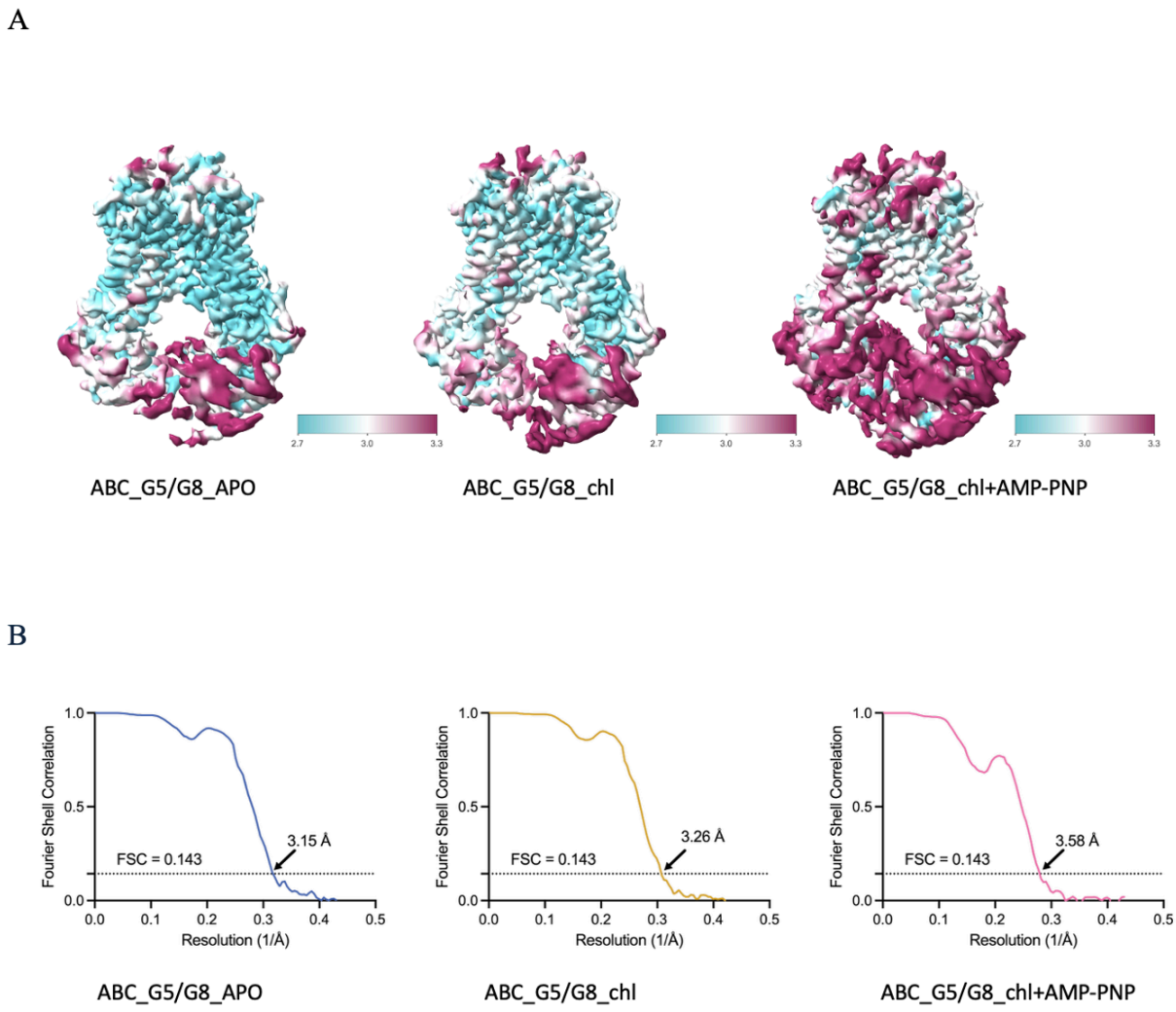

Figure 6.8. Cryo-EM map quality assessment of ABCG5/G8 in MSP1E3D1/POPC nanodisc for three sample conditions.

(A) Estimating local resolution of cryo-EM maps of ABCG5/G8 in three sample conditions, apo (ABC_G5/G8_APO), cholesterol incubated (ABC_G5/G8_chl), and cholesterol and AMPPNP incubated (ABC_G5/G8_chl+AMP-PNP), coloured according to local resolution. Colour scale from 2.7 Å (cyan, higher resolution) to 3.3 Å (magenta, lower resolution). No corresponding ligand density was resolved in any of the three maps, even after incubation with cholesterol and/or AMPPNP. In all three states, the transmembrane domains have a higher local resolution (cyan) compared to the nucleotide binding domains (magenta), which is consistent with the greater conformational flexibility of the cytoplasmic NBDs. The overall resolution range of 2.7-3.3Å indicates high quality maps in all conditions. Visualized in UCSF ChimeraX. **(B)** Gold standard Fourier Shell Correlation (FSC) curves for the three cryo-EM reconstructions. Overall resolutions of 3.15 Å, 3.26 Å, and 3.58 Å were determined for the APO, cholesterol incubated, and cholesterol and AMP-PNP incubated conditions respectively, at the FSC = 0.143 criterion (dashed line).

6.6. Density comparison across the ligand series

Single-particle cryo-EM maps of ABCG5/G8 were obtained under three experimental conditions: apo, cholesterol-incubated, and cholesterol with the non-hydrolysable ATP analogue AMP-PNP. Each sample was reconstituted in an identical MSP1E3D1/POPC nanodisc environment. The apo structure was resolved at 3.15 Å, and the three reconstructions exhibited overall resolutions ranging from approximately 3.2 to 3.6 Å **(Figure 6.9; Table 5).**

Direct comparison of the three maps at the density level revealed near-complete overlap among all conditions, as demonstrated by pairwise superposition **(Figure 6.9).** Map-to-map cross-correlation values were observed: 0.991 for apo versus +chol, 0.977 for apo versus +AMP, and 0.981 for +chol versus +AMP shown in **Table 5**. At the level of global architecture, ABCG5/G8 adopted an inward-facing conformation with separated nucleotide-binding domains. No nucleotide density was detected at the nucleotide-binding sites, including in the AMP-PNP condition. Additional non-protein density was consistently observed within the central sterol-binding cavity in all three conditions, including the apo map. The density did not increase after cholesterol was added. As the analysis was conducted at the map level without constructing an atomic model, this density remained unmodelled and was not attributed to a specific molecule.

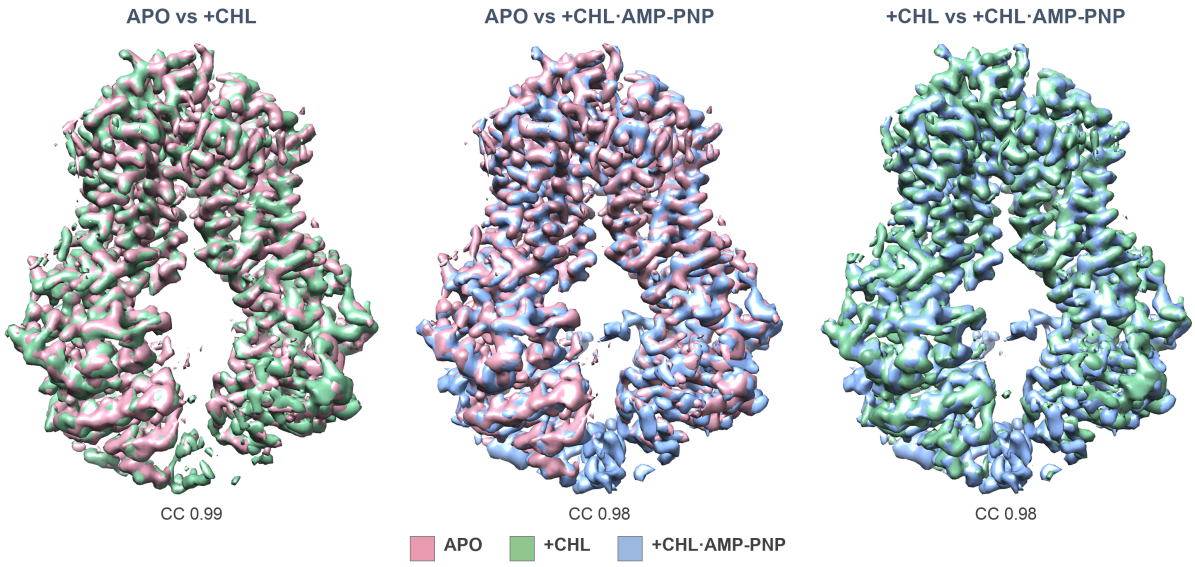

Figure 6.9. Cryo-EM map density comparison of ABCG5/G8 in MSP1E3D1/POPC nanodisc for three sample conditions.

Pairwise superpositions of ABCG5/G8 cryo-EM density maps obtained in MSP/POPC nanodiscs under three conditions: ligand-free (apo, pink), cholesterol-incubated (+CHL, green), and cholesterol plus AMP-PNP (+CHL·AMP-PNP, blue). Maps are shown at the same contour level and orientation. Left: apo versus +CHL; middle: apo versus +CHL·AMP-PNP; right: +CHL versus +CHL·AMP-PNP. Map-to-map cross-correlation values were 0.99, 0.98, and 0.98, respectively. The strong overlap and high correlation values indicate that ABCG5/G8 remains in the same inward-facing conformation under all three conditions.
Pairwise map-to-map cross-correlation (CC) between the apo, +chol, and +AMP ABCG5/G8 reconstructions.

Table 5. Pairwise map-to-map cross-correlation (CC) between the apo, +chol, and +AMP ABCG5/G8 reconstructions

Map-to-map cross-correlation (CC) coefficients were calculated between the apo, cholesterol-incubated (+chol), and cholesterol plus AMP-PNP (+AMP) reconstructions, all obtained in MSP/POPC nanodiscs. The matrix is symmetric, and self-comparisons are omitted (—). All pairwise CC values were greater than 0.97, indicating a high degree of structural similarity and supporting that ABCG5/G8 adopts the same overall inward-facing conformation under all three conditions.

CC	apo	+chol	+AMP
apo	—	0.991	0.977
+chol	0.991	—	0.981
+AMP	0.977	0.981	—

6.7. A non-protein density occupies the sterol-binding cavity in all conditions

Analysis of the central transmembrane cavity identified additional non-protein density in all three reconstructions **(Figure 6.10).** This density was observed at the established cholesterol-binding site and was present under apo, +cholesterol (CHL), and +AMP-PNP/cholesterol conditions. Upon isolation from the surrounding protein density, the feature showed a similar size and position across all three maps. As the analysis was conducted at the map level without constructing an atomic model for this density, it remained unmodelled and its molecular identity could not be determined.

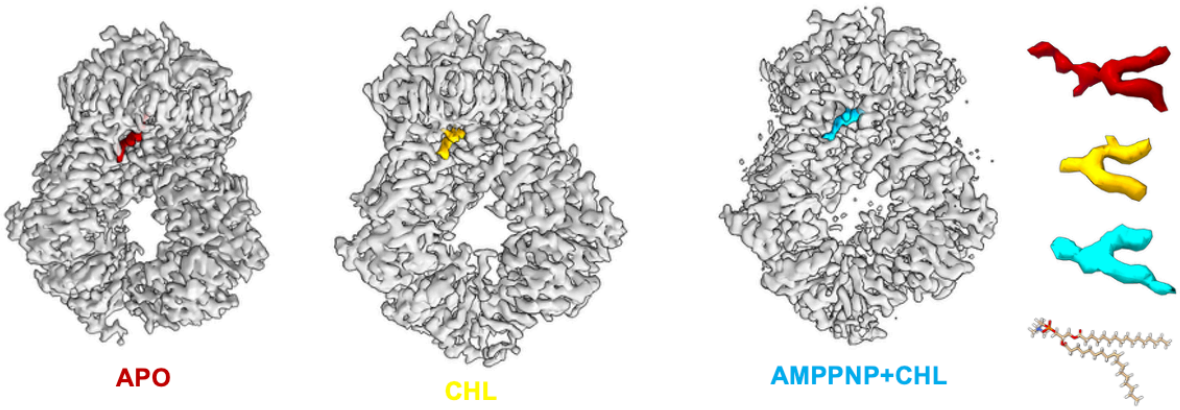

Figure 6.10 Non-protein density within the central sterol-binding cavity of ABCG5/G8 across the ligand conditions.

Cryo-EM maps (grey) of ABCG5/G8 in MSP1E3D1/POPC nanodiscs for the apo, +cholesterol (CHL), and +AMP-PNP/cholesterol conditions, with the cavity density coloured (red/yellow/cyan) and shown isolated at right. Present in all conditions including apo, the density is most consistent with a bilayer POPC; assignment is preliminary and map-level.

6.8. Nanobody Library Screening Against ABCG5/G8

6.8.1 Selection and Enrichment

To isolate nanobodies that bind to ABCG5/G8, a yeast surface display nanobody library was subjected to four rounds of magnetic bead based selection against His-tagged ABCG5/G8 purified in DDM/CHS detergent. The selection stringency increased gradually each round by decreasing the ABCG5/G8 concentration from 1 μM in Round 1 to 250 nM in Round 2, 75 nM in Round 3, and 15 nM in Round 4 in order to select the high affinity binders. Final rounds displayed a significant decrease in colony number, with approximately 300 colonies recovered after Round 3 and approximately 106 colonies after Round 4 **(Figure 6.11A)**.

6.8.2 Colony PCR and Sequencing

Following Round 4 selection, approximately 106 colonies were counted in total. The first 40 individual colonies were picked and screened by colony PCR using heat-popped yeast cells. PCR products were resolved on a 1.5% agarose gel, and of the 40 clones screened, 25 showed a band at the expected size of approximately 700 bp **(Figure 6.11B)**. The remaining 15 clones showed no amplification. Successfully amplified PCR products were sent for Sanger sequencing using the pYDS649 forward primer, and the sequences were aligned and analyzed using Benchling.

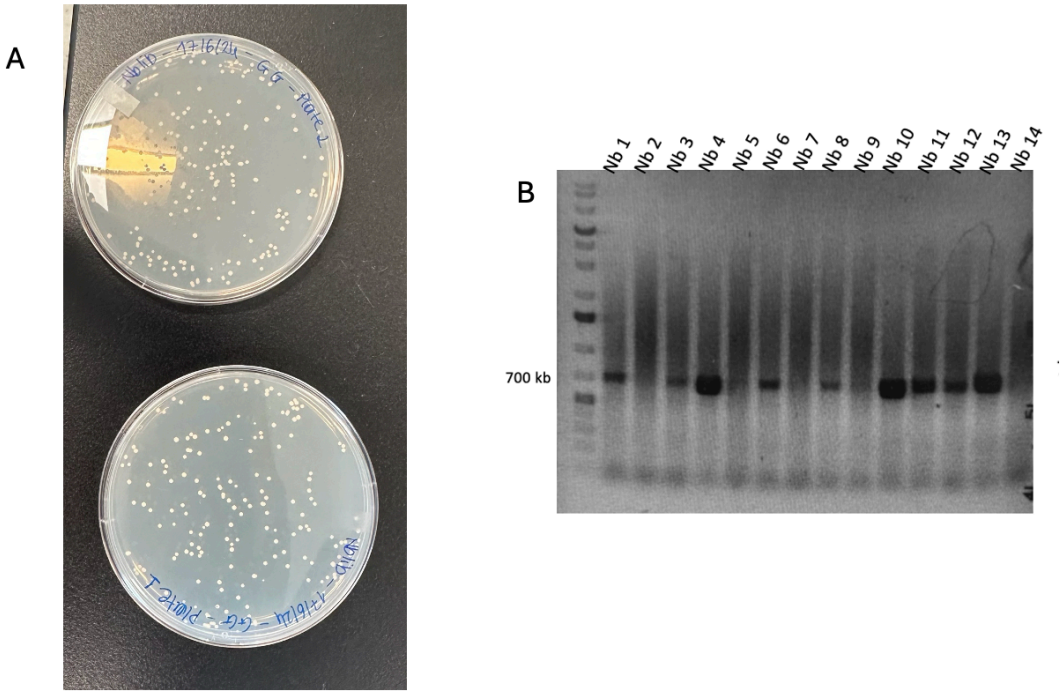

Figure 6.11. **Nanobody selection and colony PCR screening.**
(A) Representative agar plates showing yeast colonies following Round 3 magnetic bead selection at 75 nM ABCG5/G8. Approximately 300 colonies were counted across two plates. **(B)** Agarose gel (1.5%) showing colony PCR products for nanobody clones Nb1–Nb14. Bands at approximately 700 bp indicate successful amplification of the nanobody insert. A total of 40 clones were screened in this manner, of which successfully amplified products were sent for Sanger sequencing.

6.8.3 Sequence Analysis and CDR Diversity

Sequence alignment of the 25 sequenced clones revealed 5 distinct nanobody sequences, named Nb16, Nb21, Nb26, Nb29 and Nb33. The CDR1, 2 and 3 regions were aligned across all five clones using Benchling **(Figure 6.12)**. Analysis of the CDR sequences identified three distinct CDR1 sequences, GTIFHHNAM (Nb26, Nb16), GTIFYGDYM (Nb33) and GNIFRWSSM (Nb29, Nb21). Additional diversity was observed in the CDR2 and CDR3 sequences, where each clone had a unique combination of CDR sequences, suggesting that the five nanobodies might be bound to ABCG5/G8 in different binding modes though full characterization of binding modes will require resolution of the remaining CDR3 sequences, particularly for Nb26 and Nb33.

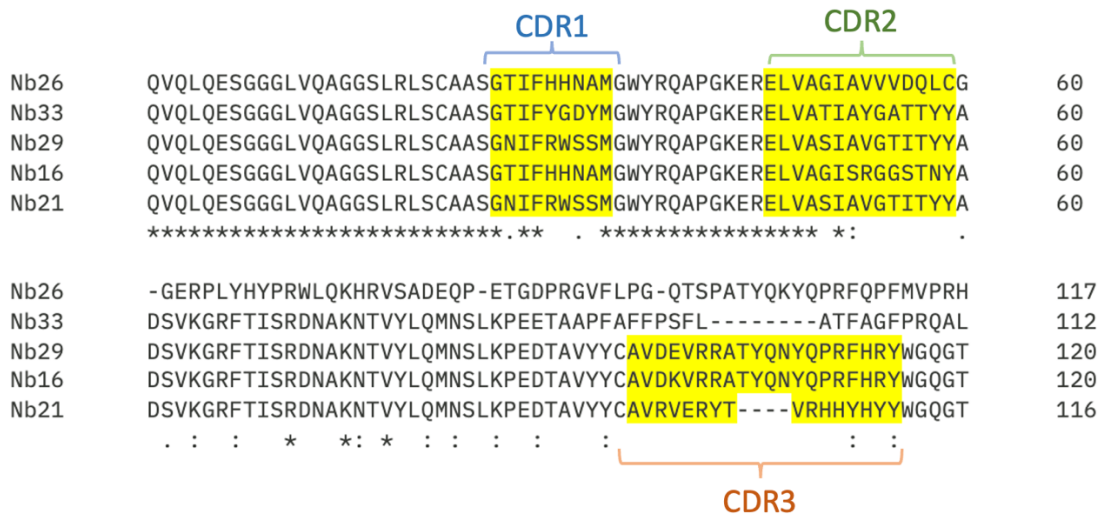

Figure 6.12. Multiple sequence alignment of five unique anti-ABCG5/G8 nanobodies.
Amino acid sequence alignment of five nanobodies (Nb26, Nb33, Nb29, Nb16, Nb21) selected from 25 nanobodies after removal of duplicate sequences. CDR1, CDR2, and CDR3 regions are highlighted in yellow. Framework regions are highly conserved (asterisks); CDR3 shows the greatest sequence and length variation. CDR3 was fully resolved for Nb29, Nb16, and Nb21 only. Alignment performed using Benchling.

7. Discussion

7.1. Expression, Purification, and Nanodisc Reconstitution of ABCG5/G8

In this study, human ABCG5/G8 was successfully expressed in *Pichia pastoris* and purified by affinity chromatography followed by size exclusion chromatography. The purified protein showed a clean monodisperse peak by SEC, and the expected two bands at ~ 75 kDa by SDS-PAGE confirming the integrity of the heterodimer. MSP1D1 expression and purification was also optimized to yield large quantities (40 mg) of MSP, and the same protocol was subsequently used to obtain even more MSP1E3D1 (60 mg). These optimized protocols provided a reliable source of both MSP and ABCG5/G8 for downstream applications, easing one of the practical limitations for nanodisc based structural studies.

An important part of this work was the systematic investigation of conditions for nanodisc reconstitution. Four combinations of MSP (MSP1D1 and MSP1E3D1) and lipid (POPC and *E. coli* polar lipid extract) were tested and sample homogeneity, grid quality and particle distribution were evaluated at multiple stages of the workflow. Although all four conditions yielded acceptable SEC profiles consistent with successful reconstitution, grid screening revealed differences in the quality of the particles across conditions. The conditions made with MSP1D1 resulted in low particle density on the grids, preventing further data collection. In contrast, the two MSP1E3D1 based conditions resulted in grids with well distributed particles, suitable for cryo-EM data collection. Therefore, Cryo-EM data was collected for both MSP1E3D1/POPC and MSP1E3D1/E. coli nanodiscs. However, initial 2D classification of MSP1E3D1/*E. coli* nanodiscs resulted in low resolution class averages with poorly defined features, potentially indicating conformational flexibility of the protein in *E. coli* lipids environment. Finally, only the MSP1E3D1/POPC dataset

resulted in 2D class averages with structural details sufficient for a high-resolution 3D reconstruction during data processing.

The effect of scaffold size under identical lipid conditions was assessed by reconstituting ABCG5/G8 in POPC nanodiscs using either MSP1D1 or MSP1E3D1. These scaffold proteins primarily differ in the diameter of the nanodiscs they form: MSP1D1 generates discs approximately ~9.7 nm in diameter, while MSP1E3D1 forms larger discs of about ~12.9 nm and incorporates more lipid **(Table 6)**. As both conditions utilized POPC, bilayer thickness remained consistent, with the principal variable being the lateral space surrounding ABCG5/G8. The smaller MSP1D1/POPC nanodiscs yielded fewer well-behaved particles, whereas the larger MSP1E3D1/POPC nanodiscs provided increased space around the transporter and resulted in more uniform particles suitable for cryo-EM analysis. Therefore, under POPC conditions, MSP1E3D1 was more suitable for ABCG5/G8 than MSP1D1.

Table 6. MSP scaffold comparison

Comparison of the two membrane scaffold proteins tested for ABCG5/G8 nanodisc reconstitution. The two scaffolds differ in disc diameter and lipid capacity[61].

Property	MSP1D1	MSP1E3D1
Disc diameter	~9.7 nm	~12.9 nm
POPC per disc	~130	~260
Annular lipid area	Smaller	Larger
Suitability for ABCG5/G8 (~150 kDa)	Too crowded	Seats the dimer + lipid shell

To compare lipid composition under identical scaffold conditions, ABCG5/G8 was reconstituted in MSP1E3D1 nanodiscs containing either POPC or E. coli polar lipid extract. Although both lipid environments have a similar overall bilayer thickness, they differ in composition, charge, and curvature. POPC is a single, defined zwitterionic phospholipid, while E. coli polar lipid extract is a complex mixture containing phosphatidylethanolamine, phosphatidylglycerol, and cardiolipin **(Table 7).** As a result, POPC provided a simpler and more reproducible membrane environment. The MSP1E3D1/POPC condition yielded well-defined 2D class averages suitable for high-resolution reconstruction, whereas the MSP1E3D1/E. coli lipid condition gave poorer 2D classes. This may reflect greater heterogeneity in the E. coli lipid mixture, although this was not investigated further.

Table 7. Lipid comparison

POPC and *E.coli* polar lipid extract[85] are well matched in bilayer hydrophobic thickness but differ substantially in surface charge and spontaneous curvature. Only the MSP1E3D1/POPC combination yielded class averages suitable for high-resolution reconstruction[86].

Property	POPC	*E.coli* polar lipid extract
Composition	Single defined lipid (16:0/18:1PC)	Mixture (PE ~67%, PG ~23.2%, cardiolipin ~9.8%)
Hydrophobic thickness	~27 Å	~27 Å
Net surface charge	Zwitterionic (neutral)	~33% anionic
Spontaneous curvature	~flat (cylindrical)	Negative (cone-shaped PE + cardiolipin)
Cryo-EM outcome	High-resolution 2D classes → 3D reconstruction	Low-resolution, poorly defined 2D classes

The scaffold and lipid conditions evaluated in this study represent only a small part of the possible nanodisc design space. For the scaffold, disc size is an important factor because it determines how much lipid surrounds the ABCG5/G8 heterodimer. Smaller scaffolds, such as MSP1D1 and MSP1D1ΔH5, may provide insufficient space, while larger scaffolds, such as MSP2N2, may introduce excess lipid and increase heterogeneity. Intermediate-sized scaffolds, including MSP1E1D1 or MSP1E2D1, as well as circularized nanodiscs, could therefore be tested in future studies. Alternative membrane-mimetic systems, such as saposin-based particles or peptidiscs could also be considered **(Table 8).**

Table 8. Comparison of membrane scaffold system options for ABCG5/G8 nanodisc reconstitution

Scaffold	Disc diameter	Fit / trade-off
MSP1D1ΔH5	~8.4	Too tight
MSP1D1	~9.7	Crowding / heterogenous
MSP1E1D1 / E2D1	~10.6 / 11.9	Untested middle ground
MSP1E3D1	~12.9	Used / best: good annulus, monodisperse
MSP2N2	~16–17	Larger, but more off-target lipid density
Circularized MSP[87]	~11 / ~15	Future: more homogeneous / thermostable
Saposin A[88]	adaptive	Zhang 2021; less defined than MSP
Peptidisc[89]	adaptive	Native-lipid options; composition less defined

Lipid composition could also be explored further. POPC was used here because it provides a simple and reproducible membrane environment; however, defined lipid mixtures could be used to test specific membrane properties. For instance, POPG may introduce negative charge, POPE could influence membrane curvature, and cholesterol or sphingomyelin: cholesterol mixtures might yield a more physiologically relevant environment. However, adding cholesterol in the nanodisc would complicate studies aimed at identifying sterol binding within ABCG5/G8 **(Table 9)**. Overall, MSP1E3D1/POPC provided a suitable balance between sufficient space around ABCG5/G8 and maintaining a simple, homogeneous lipid environment, though further optimization may improve the system.

Table 9. Comparison of lipid options for ABCG5/G8 nanodisc reconstitution

Lipid/system	Key feature	Verdict
POPC	Fluid, zwitterionic	Chosen: defined, fluid, reproducible
POPC:POPG	Adds negative charge	May improve assembly
POPC:POPE	Negative curvature	Tests curvature
POPC:cholesterol	Sterol-rich	Native-like, but confounds ligand
POPC:SM:chol	Raft-like	Most physiological; hardest to reproduce
E. coli polar extract	PE/PG/CL mix	Tested: heterogeneous, non-mammalian

7.2. Cryo-EM Structural Studies of ABCG5/G8

The optimized MSP1E3D1/POPC nanodisc system allowed determination of cryo-EM structures of ABCG5/G8 in three sample conditions: apo, cholesterol incubated, and cholesterol- and AMP-PNP incubated. The apo reconstruction resulted in an overall resolution of 3.15 Å, with similar resolutions of 3.26 Å and 3.58 Å for the cholesterol and cholesterol+AMP-PNP datasets, respectively. These are the first cryo-EM structures of ABCG5/G8 reconstituted in MSP nanodiscs and demonstrate that the optimized sample preparation protocol developed in this thesis yields particles of sufficient quality to allow high resolution structural analysis.

All three reconstructions reveal ABCG5/G8 in an inward-facing, nucleotide-free conformation. This observation is consistent with previously reported ABCG5/G8 structures[35,36,44,53] including apo, cholesterol-bound, and earlier cryo-EM structures, which have also captured the transporter in an inward-facing state. Observing the same overall conformation under three different conditions and in MSP/POPC nanodiscs indicates that it represents a stable resting state of the transporter, rather than an artifact of a specific membrane-mimetic system. In this conformation, the transmembrane cavity is open toward the cytoplasmic side of the membrane, which aligns with a substrate-accepting state before ATP-driven transport. Capturing this state in a defined lipid bilayer provides a robust system for investigating the mechanisms by which ABCG5/G8 recognizes sterols and how this process may be altered in sitosterolemia.

No significant conformational differences were observed between the three reconstructions, and pairwise map-to-map cross-correlation values remained uniformly high (≥ 0.977). This result is informative rather than simply negative. Because the conformational switch of ABCG5/G8 is regulated by nucleotide binding and hydrolysis at the nucleotide-binding domains, rather than by substrate binding, cholesterol alone would not be expected to induce a conformational change. The lack of structural change in the cholesterol condition aligns with this mechanism. Furthermore, the observation that the transporter did not adopt a nucleotide-bound, closed state in the presence of AMP-PNP indicates that the analogue did not stably engage the nucleotide-binding domains under the incubation conditions used. This may reflect incubation times or ligand concentrations to fully populate a distinct state, or the requirement for additional factors such as magnesium, a transition-state mimic, or a catalytically inactivating mutation to stabilize an intermediate state.

Non-protein density was observed within the central transmembrane cavity at the established cholesterol-binding site in all three reconstructions. As this density was present in the apo condition and did not increase following cholesterol addition, it is unlikely to represent only the supplemented cholesterol. Given that ABCG5/G8 was reconstituted in POPC nanodiscs, the density may correspond to a POPC molecule occupying the cavity. This interpretation remains preliminary because no atomic model was built for the density and no significant difference density was observed between experimental conditions. Consequently, the feature is best characterized as unassigned density at the sterol-binding site rather than definitive evidence of sterol binding.

While the absence of a captured intermediate is a limitation, the development of a workflow that yields high-resolution cryo-EM data of ABCG5/G8 in a native-like lipid environment is an important achievement. Future work should focus on improving ligand delivery and stabilizing additional conformational states. Potential strategies include increasing cholesterol loading, optimizing incubation conditions, employing nucleotide or transition-state analogues, and introducing hydrolysis-deficient mutations to facilitate the trapping of intermediate states.

Beyond improving ligand and nucleotide trapping, the nanodisc system itself could also be optimized further. Intermediate-sized scaffolds, such as MSP1E1D1 and MSP1E2D1, circularized nanodiscs, or alternative systems including saposin A and peptidiscs, may be evaluated to improve particle homogeneity and stability. Lipid composition could also be varied systematically to examine how membrane properties influence ABCG5/G8. For instance, POPG-containing mixtures can assess the effect of negative charge, POPE-containing mixtures can examine membrane curvature, and cholesterol- or sphingomyelin-containing mixtures can provide a more physiologically relevant environment. Because the system established here allows both scaffold

and lipid composition to be changed independently, it provides a useful platform for future optimization and mechanistic studies.

7.3. Identification of ABCG5/G8 Specific Nanobodies

In parallel to the structural studies, a yeast surface display nanobody library was screened to identify ABCG5/G8 specific binders. Following 4 rounds of magnetic bead based selection at decreasing antigen concentrations, a clear enrichment of binders was observed in **Figure 6.11** with colony counts decreasing from too many to count after Round 1 and Round 2, to about 300 colonies after Round 3 and 80 colonies after Round 4. Five unique nanobody sequences (Nb16, Nb21, Nb26, Nb29 and Nb33) were identified by Sanger sequencing of 25 individual clones, with sequence alignment showing three different CDR1 families, four different CDR2 and unique CDR3 sequences. The presence of binders that recognize distinct sites increase the likelihood that at least one will be applicable in future contexts, including stabilizing a specific conformation, serving as a cryo-EM fiducial, or targeting a functionally important region.

So far, these are the first reported ABCG5/G8 specific nanobodies. The identification of these binders provides new molecular tools to study ABCG5/G8 and may provide a starting point for future structural and therapeutic investigations. The small size of nanobodies and their ability to bind hidden or conformation specific epitopes makes them particularly attractive tools for stabilizing distinct conformational states of ABCG5/G8, they can also be useful as cryo-EM fiducial markers. This approach may be particularly advantageous for ABCG5/G8, as its pseudo-symmetric membrane-embedded structure offers few distinct features for particle alignment. The presence of a bound nanobody could introduce asymmetry and enhance particle orientation during image processing. Additionally, nanobodies that preferentially bind specific conformations may

stabilize transport states not observed in the present study and facilitate further investigation of the ABCG5/G8 catalytic cycle.

A limitation of this study is that the nanobodies have been identified solely through sequencing. Their binding affinity, specificity, and impact on ABCG5/G8 function have not yet been characterized, and it is unclear whether they interact effectively with the transporter in a lipid environment. Future work should therefore include recombinant expression and purification of the candidate nanobodies, followed by binding measurements using techniques such as surface plasmon resonance. The effects of these nanobodies on ABCG5/G8 activity should be evaluated using ATPase and sterol-transport assays. Promising candidates may be complexed with ABCG5/G8 in nanodiscs for cryo-electron microscopy studies, which could facilitate stabilization of distinct conformational states or elucidate the influence of nanobody binding on transporter function. Well-characterized nanobodies that modulate ABCG5/G8 activity may serve as valuable tools for investigating sterol transport and, ultimately, for assessing the transporter as a potential therapeutic target.

7.4. Concluding Remarks

Overall, the work presented in this thesis contributes to the structural biology and molecular tools available to study ABCG5/G8. A workflow was established for the expression, purification, and reconstitution of ABCG5/G8 into nanodiscs, which enabled high resolution cryo-EM structure determination in a native like lipid bilayer environment. Screening of different sample conditions further identified conditions that can be used for future structural studies of ABCG5/G8. At the same time, the identification of five specific ABCG5/G8 binding nanobodies for future biochemical and cryo-EM studies, with potential applications as structural tools or as

candidates for further development as transporter modulators. Together, these findings provide a foundation for work aimed at understanding the molecular mechanism of sterol transport by ABCG5/G8 and may support the long term development of targeted approaches for sitosterolemia and related cholesterol metabolism disorders.

8. References

1. Steck, T. L., & Lange, Y. (2018). Transverse distribution of plasma membrane bilayer cholesterol: Picking sides. *Traffic*, *19*(10), 750–760. https://doi.org/10.1111/tra.12586
2. Yang, S.-T., Kreutzberger, A. J. B., Lee, J., Kiessling, V., & Tamm, L. K. (2016). The Role of Cholesterol in Membrane Fusion. *Chemistry and Physics of Lipids*, *199*, 136–143. https://doi.org/10.1016/j.chemphyslip.2016.05.003
3. Li, T., & Chiang, J. Y. L. (2009). Regulation of Bile Acid and Cholesterol Metabolism by PPARs. *PPAR Research*, *2009*, 501739. https://doi.org/10.1155/2009/501739
4. Lingwood, D., & Simons, K. (2010). Lipid Rafts As a Membrane-Organizing Principle. *Science*, *327*(5961), 46–50. https://doi.org/10.1126/science.1174621
5. Rezaei, F., Farhat, D., Gursu, G., Samnani, S., & Lee, J.-Y. (2023). Snapshots of ABCG1 and ABCG5/G8: A Sterol's Journey to Cross the Cellular Membranes. *International Journal of Molecular Sciences*, *24*(1), Article 1. https://doi.org/10.3390/ijms24010484
6. Wang, D. Q.-H. (2007). Regulation of Intestinal Cholesterol Absorption. *Annual Review of Physiology*, *69*, 221–248. https://doi.org/10.1146/annurev.physiol.69.031905.160725
7. Maxfield, F. R., & Tabas, I. (2005). Role of cholesterol and lipid organization in disease. *Nature*, *438*(7068), 612–621. https://doi.org/10.1038/nature04399
8. Istvan, E. S., & Deisenhofer, J. (2001). Structural Mechanism for Statin Inhibition of HMG-CoA Reductase. *Science*, *292*(5519), 1160–1164. https://doi.org/10.1126/science.1059344

9. Goldstein, J. L., & Brown, M. S. (2015). A Century of Cholesterol and Coronaries: From Plaques to Genes to Statins. *Cell*, *161*(1), 161–172. https://doi.org/10.1016/j.cell.2015.01.036
10. Nissen, S. E., Lincoff, A. M., Brennan, D., Ray, K. K., Mason, D., Kastelein, J. J. P., Thompson, P. D., Libby, P., Cho, L., Plutzky, J., Bays, H. E., Moriarty, P. M., Menon, V., Grobbee, D. E., Louie, M. J., Chen, C.-F., Li, N., Bloedon, L., Robinson, P., … Nicholls, S. J. (2023). Bempedoic Acid and Cardiovascular Outcomes in Statin-Intolerant Patients. *New England Journal of Medicine*, *388*(15), 1353–1364. https://doi.org/10.1056/NEJMoa2215024
11. Ray, K. K., Molemans, B., Schoonen, W. M., Giovas, P., Bray, S., Kiru, G., Murphy, J., Banach, M., De Servi, S., Gaita, D., Gouni-Berthold, I., Hovingh, G. K., Jozwiak, J. J., Jukema, J. W., Kiss, R. G., Kownator, S., Iversen, H. K., Maher, V., Masana, L., … the DA VINCI study. (2021). EU-Wide Cross-Sectional Observational Study of Lipid-Modifying Therapy Use in Secondary and Primary Care: The DA VINCI study. *European Journal of Preventive Cardiology*, *28*(11), 1279–1289. https://doi.org/10.1093/eurjpc/zwaa047
12. Valsta, L. M., Lemström, A., Ovaskainen, M.-L., Lampi, A.-M., Toivo, J., Korhonen, T., & Piironen, V. (2004). Estimation of plant sterol and cholesterol intake in Finland: Quality of new values and their effect on intake. *British Journal of Nutrition*, *92*(4), 671–678. https://doi.org/10.1079/BJN20041234
13. Salen, G., Patel, S., & Batta, A. K. (2002). Sitosterolemia. *Cardiovascular Drug Reviews*, *20*(4), 255–270. https://doi.org/10.1111/j.1527-3466.2002.tb00096.x

14. Bydlowski, S. P., & Levy, D. (2024). Association of ABCG5 and ABCG8 Transporters with Sitosterolemia. In G. Lizard (Ed.), *Implication of Oxysterols and Phytosterols in Aging and Human Diseases* (pp. 31–42). Springer International Publishing. https://doi.org/10.1007/978-3-031-43883-7_2
15. Luo, J., Yang, H., & Song, B.-L. (2020). Mechanisms and regulation of cholesterol homeostasis. *Nature Reviews Molecular Cell Biology*, *21*(4), 225–245. https://doi.org/10.1038/s41580-019-0190-7
16. Vrins, C. L. J., Ottenhoff, R., van den Oever, K., de Waart, D. R., Kruyt, J. K., Zhao, Y., van Berkel, T. J. C., Havekes, L. M., Aerts, J. M., van Eck, M., Rensen, P. C. N., & Groen, A. K. (2012). Trans-intestinal cholesterol efflux is not mediated through high density lipoprotein. *Journal of Lipid Research*, *53*(10), 2017–2023. https://doi.org/10.1194/jlr.M022194
17. Ouimet, M., Barrett, T. J., & Fisher, E. A. (2019). HDL and Reverse Cholesterol Transport. *Circulation Research*, *124*(10), 1505–1518. https://doi.org/10.1161/CIRCRESAHA.119.312617
18. Li, G., Gu, H.-M., & Zhang, D.-W. (2013). ATP-binding cassette transporters and cholesterol translocation. *IUBMB Life*, *65*(6), 505–512. https://doi.org/10.1002/iub.1165
19. van der Velde, A. E., Vrins, C. L. J., van den Oever, K., Kunne, C., Oude Elferink, R. P. J., Kuipers, F., & Groen, A. K. (2007). Direct Intestinal Cholesterol Secretion Contributes Significantly to Total Fecal Neutral Sterol Excretion in Mice. *Gastroenterology*, *133*(3), 967–975. https://doi.org/10.1053/j.gastro.2007.06.019

20. Jakulj, L., Dijk, T. H. van, Boer, J. F. de, Kootte, R. S., Schonewille, M., Paalvast, Y., Boer, T., Bloks, V. W., Boverhof, R., Nieuwdorp, M., Beuers, U. H. W., Stroes, E. S. G., & Groen, A. K. (2016). Transintestinal Cholesterol Transport Is Active in Mice and Humans and Controls Ezetimibe-Induced Fecal Neutral Sterol Excretion. *Cell Metabolism*, *24*(6), 783–794. https://doi.org/10.1016/j.cmet.2016.10.001
21. Plummer, A. M., Culbertson, A. T., & Liao, M. (2021). The ABCs of Sterol Transport. *Annual Review of Physiology*, *83*(Volume 83, 2021), 153–181. https://doi.org/10.1146/annurev-physiol-031620-094944
22. Ristovski, M., Farhat, D., Bancud, S. E. M., & Lee, J.-Y. (2021). Lipid Transporters Beam Signals from Cell Membranes. *Membranes*, *11*(8), 562. https://doi.org/10.3390/membranes11080562
23. Dean, M., Hamon, Y., & Chimini, G. (2001). The human ATP-binding cassette (ABC) transporter superfamily. *Journal of Lipid Research*, *42*(7), 1007–1017.
24. Beis, K. (2015). Structural basis for the mechanism of ABC transporters. *Biochemical Society Transactions*, *43*(5), 889–893. https://doi.org/10.1042/BST20150047
25. Locher, K. P. (2016). Mechanistic diversity in ATP-binding cassette (ABC) transporters. *Nature Structural & Molecular Biology*, *23*(6), 487–493. https://doi.org/10.1038/nsmb.3216
26. Liu, X. (2019). ABC Family Transporters. In X. Liu & G. Pan (Eds.), *Drug Transporters in Drug Disposition, Effects and Toxicity* (pp. 13–100). Springer. https://doi.org/10.1007/978-981-13-7647-4_2

27. Xavier, B. M., Jennings, W. J., Zein, A. A., Wang, J., & Lee, J.-Y. (2019). Structural snapshot of the cholesterol-transport ATP-binding cassette proteins. *Biochemistry and Cell Biology*, *97*(3), 224–233. https://doi.org/10.1139/bcb-2018-0151

28. Tarr, P. T., Tarling, E. J., Bojanic, D. D., Edwards, P. A., & Baldán, Á. (2009). Emerging new paradigms for ABCG transporters. *Biochimica et Biophysica Acta (BBA) - Molecular and Cell Biology of Lipids, Cellular Lipid Transport Processes and Their Role in Human Disease*, *1791*(7), 584–593. https://doi.org/10.1016/j.bbalip.2009.01.007

29. Graf, G. A., Yu, L., Li, W.-P., Gerard, R., Tuma, P. L., Cohen, J. C., & Hobbs, H. H. (2003). ABCG5 and ABCG8 Are Obligate Heterodimers for Protein Trafficking and Biliary Cholesterol Excretion *. *Journal of Biological Chemistry*, *278*(48), 48275–48282. https://doi.org/10.1074/jbc.M310223200

30. Berge, K. E., Tian, H., Graf, G. A., Yu, L., Grishin, N. V., Schultz, J., Kwiterovich, P., Shan, B., Barnes, R., & Hobbs, H. H. (2000). Accumulation of Dietary Cholesterol in Sitosterolemia Caused by Mutations in Adjacent ABC Transporters. *Science*, *290*(5497), 1771–1775. https://doi.org/10.1126/science.290.5497.1771

31. Sumi, K., Tanaka, T., Uchida, A., Magoori, K., Urashima, Y., Ohashi, R., Ohguchi, H., Okamura, M., Kudo, H., Daigo, K., Maejima, T., Kojima, N., Sakakibara, I., Jiang, S., Hasegawa, G., Kim, I., Osborne, T. F., Naito, M., Gonzalez, F. J., … Sakai, J. (2007). Cooperative Interaction between Hepatocyte Nuclear Factor 4α and GATA Transcription Factors Regulates ATP-Binding Cassette Sterol Transporters ABCG5 and ABCG8. *Molecular and Cellular Biology*, *27*(12), 4248–4260. https://doi.org/10.1128/MCB.01894-06

32. Freeman, L. A., Kennedy, A., Wu, J., Bark, S., Remaley, A. T., Santamarina-Fojo, S., & Brewer, H. B. (2004). The orphan nuclear receptor LRH-1 activates the ABCG5/ABCG8 intergenic promoter. *Journal of Lipid Research*, *45*(7), 1197–1206. https://doi.org/10.1194/jlr.C400002-JLR200

33. Repa, J. J., Berge, K. E., Pomajzl, C., Richardson, J. A., Hobbs, H., & Mangelsdorf, D. J. (2002). Regulation of ATP-binding Cassette Sterol Transporters ABCG5 and ABCG8 by the Liver X Receptors α and β*. *Journal of Biological Chemistry*, *277*(21), 18793–18800. https://doi.org/10.1074/jbc.M109927200

34. Graf, G. A., Li, W.-P., Gerard, R. D., Gelissen, I., White, A., Cohen, J. C., & Hobbs, H. H. (2002). Coexpression of ATP-binding cassette proteins ABCG5 and ABCG8 permits their transport to the apical surface. *The Journal of Clinical Investigation*, *110*(5), 659–669. https://doi.org/10.1172/JCI16000

35. Lee, J.-Y., Kinch, L. N., Borek, D. M., Wang, J., Wang, J., Urbatsch, I. L., Xie, X.-S., Grishin, N. V., Cohen, J. C., Otwinowski, Z., Hobbs, H. H., & Rosenbaum, D. M. (2016). Crystal structure of the human sterol transporter ABCG5/ABCG8. *Nature*, *533*(7604), Article 7604. https://doi.org/10.1038/nature17666

36. Farhat, D., Rezaei, F., Ristovski, M., Yang, Y., Stancescu, A., Dzimkova, L., Samnani, S., Couture, J.-F., & Lee, J.-Y. (2022). Structural Analysis of Cholesterol Binding and Sterol Selectivity by ABCG5/G8. *Journal of Molecular Biology*, *434*(20), 167795. https://doi.org/10.1016/j.jmb.2022.167795

37. Patel, S. B., Graf, G. A., & Temel, R. E. (2018). Thematic Review Series: Lipid Transfer Proteins ABCG5 and ABCG8: more than a defense against xenosterols. *Journal of Lipid Research*, *59*(7), 1103–1113. https://doi.org/10.1194/jlr.R084244

38. Yu, L., Hammer, R. E., Li-Hawkins, J., von Bergmann, K., Lutjohann, D., Cohen, J. C., & Hobbs, H. H. (2002). Disruption of Abcg5 and Abcg8 in mice reveals their crucial role in biliary cholesterol secretion. *Proceedings of the National Academy of Sciences of the United States of America*, *99*(25), 16237–16242. https://doi.org/10.1073/pnas.252582399

39. Zein, A. A., Kaur, R., Hussein, T. O. K., Graf, G. A., & Lee, J.-Y. (2019). ABCG5/G8: A structural view to pathophysiology of the hepatobiliary cholesterol secretion. *Biochemical Society Transactions*, *47*(5), 1259–1268. https://doi.org/10.1042/BST20190130

40. Phillips, M. C. (2014). Molecular Mechanisms of Cellular Cholesterol Efflux. *The Journal of Biological Chemistry*, *289*(35), 24020–24029. https://doi.org/10.1074/jbc.R114.583658

41. Hubacek, J. A., Berge, K. E., Cohen, J. C., & Hobbs, H. H. (2001). Mutations in ATP-cassette binding proteins G5 (ABCG5) and G8 (ABCG8) causing sitosterolemia. *Human Mutation*, *18*(4), 359–360. https://doi.org/10.1002/humu.1206

42. Berge, K. E., Tian, H., Graf, G. A., Yu, L., Grishin, N. V., Schultz, J., Kwiterovich, P., Shan, B., Barnes, R., & Hobbs, H. H. (2000). Accumulation of dietary cholesterol in sitosterolemia caused by mutations in adjacent ABC transporters. *Science (New York, N.Y.)*, *290*(5497), 1771–1775. https://doi.org/10.1126/science.290.5497.1771

43. Kidambi, S., & Patel, S. B. (2008). Sitosterolaemia: Pathophysiology, clinical presentation and laboratory diagnosis. *Journal of Clinical Pathology*, *61*(5), 588–594. https://doi.org/10.1136/jcp.2007.049775

44. Sun, Y., Wang, J., Long, T., Qi, X., Donnelly, L., Elghobashi-Meinhardt, N., Esparza, L., Cohen, J. C., Xie, X.-S., Hobbs, H. H., & Li, X. (2021). Molecular basis of cholesterol efflux via ABCG subfamily transporters. *Proceedings of the National Academy of Sciences of the United States of America*, *118*(34), e2110483118. https://doi.org/10.1073/pnas.2110483118

45. Neifert, A. R., Su, D., Ochoa Chaar, C. I., & Sumpio, B. E. (2023). Premature atherosclerosis: A review of current literature. *JVS-Vascular Insights*, *1*, 100013. https://doi.org/10.1016/j.jvsvi.2023.100013

46. Lee, M.-H., Lu, K., Hazard, S., Yu, H., Shulenin, S., Hidaka, H., Kojima, H., Allikmets, R., Sakuma, N., Pegoraro, R., Srivastava, A. K., Salen, G., Dean, M., & Patel, S. B. (2001). Identification of a gene, ABCG5, important in the regulation of dietary cholesterol absorption. *Nature Genetics*, *27*(1), Article 1. https://doi.org/10.1038/83799

47. Guay, S.-P., Paquette, M., Blais, C., Gosse, G., & Baass, A. (2024). Two Cases of Sitosterolemia Falsely Diagnosed as Familial Hypercholesterolemia: Could Digging Deeper Have Avoided Harm? *JCEM Case Reports*, *2*(5), luae086. https://doi.org/10.1210/jcemcr/luae086

48. Nordestgaard, B. G., Chapman, M. J., Humphries, S. E., Ginsberg, H. N., Masana, L., Descamps, O. S., Wiklund, O., Hegele, R. A., Raal, F. J., Defesche, J. C., Wiegman, A., Santos, R. D., Watts, G. F., Parhofer, K. G., Hovingh, G. K., Kovanen, P. T., Boileau, C.,

Averna, M., Borén, J., … for the European Atherosclerosis Society Consensus Panel. (2013). Familial hypercholesterolaemia is underdiagnosed and undertreated in the general population: Guidance for clinicians to prevent coronary heart disease : Consensus Statement of the European Atherosclerosis Society. *European Heart Journal*, *34*(45), 3478–3490. https://doi.org/10.1093/eurheartj/eht273

49. Tada, H., Nohara, A., Inazu, A., Sakuma, N., Mabuchi, H., & Kawashiri, M. (2018). Sitosterolemia, Hypercholesterolemia, and Coronary Artery Disease. *Journal of Atherosclerosis and Thrombosis*, *25*(9), 783–789. https://doi.org/10.5551/jat.RV17024
50. Tada, H., Nomura, A., Ogura, M., Ikewaki, K., Ishigaki, Y., Inagaki, K., Tsukamoto, K., Dobashi, K., Nakamura, K., Hori, M., Matsuki, K., Yamashita, S., Yokoyama, S., Kawashiri, M., & Harada-Shiba, M. (2021). Diagnosis and Management of Sitosterolemia 2021. *Journal of Atherosclerosis and Thrombosis*, *28*(8), 791–801. https://doi.org/10.5551/jat.RV17052
51. Stender, S., Frikke-Schmidt, R., Nordestgaard, B. G., & Tybjærg-Hansen, A. (2014). The ABCG5/8 Cholesterol Transporter and Myocardial Infarction Versus Gallstone Disease. *Journal of the American College of Cardiology*, *63*(20), 2121–2128. https://doi.org/10.1016/j.jacc.2013.12.055
52. Xavier, B. M., Zein, A. A., Venes, A., Wang, J., & Lee, J.-Y. (2020). Transmembrane Polar Relay Drives the Allosteric Regulation for ABCG5/G8 Sterol Transporter. *International Journal of Molecular Sciences*, *21*(22), 8747. https://doi.org/10.3390/ijms21228747

53. Zhang, H., Huang, C.-S., Yu, X., Lee, J., Vaish, A., Chen, Q., Zhou, M., Wang, Z., & Min, X. (2021). Cryo-EM structure of ABCG5/G8 in complex with modulating antibodies. *Communications Biology*, *4*(1), Article 1. https://doi.org/10.1038/s42003-021-02039-8

54. Denisov, I. G., & Sligar, S. G. (2016). Nanodiscs for structural and functional studies of membrane proteins. *Nature Structural & Molecular Biology*, *23*(6), Article 6. https://doi.org/10.1038/nsmb.3195

55. Pettersen, J. M., Yang, Y., & Robinson, A. S. (2023). Advances in nanodisc platforms for membrane protein purification. *Trends in Biotechnology*, *41*(8), 1041–1054. https://doi.org/10.1016/j.tibtech.2023.02.006

56. Carpenter, E. P., Beis, K., Cameron, A. D., & Iwata, S. (2008). Overcoming the challenges of membrane protein crystallography. *Current Opinion in Structural Biology, Carbohydrates and Glycoconjugates / Biophysical Methods*, *18*(5), 581–586. https://doi.org/10.1016/j.sbi.2008.07.001

57. Bayburt, T. H., Grinkova, Y. V., & Sligar, S. G. (2002). Self-Assembly of Discoidal Phospholipid Bilayer Nanoparticles with Membrane Scaffold Proteins. *Nano Letters*, *2*(8), 853–856. https://doi.org/10.1021/nl025623k

58. Bayburt, T. H., & Sligar, S. G. (2003). Self-assembly of single integral membrane proteins into soluble nanoscale phospholipid bilayers. *Protein Science : A Publication of the Protein Society*, *12*(11), 2476–2481.

59. Denisov, I. G., Grinkova, Y. V., Lazarides, A. A., & Sligar, S. G. (2004). Directed Self-Assembly of Monodisperse Phospholipid Bilayer Nanodiscs with Controlled Size. *Journal*

of the American Chemical Society, *126*(11), 3477–3487. https://doi.org/10.1021/ja0393574

60. Grinkova, Y. V., Denisov, I. G., & Sligar, S. G. (2010). Engineering extended membrane scaffold proteins for self-assembly of soluble nanoscale lipid bilayers. *Protein Engineering, Design and Selection*, *23*(11), 843–848. https://doi.org/10.1093/protein/gzq060
61. Ritchie, T. K., Grinkova, Y. V., Bayburt, T. H., Denisov, I. G., Zolnerciks, J. K., Atkins, W. M., & Sligar, S. G. (2009). Reconstitution of Membrane Proteins in Phospholipid Bilayer Nanodiscs. *Methods in Enzymology*, *464*, 211–231. https://doi.org/10.1016/S0076-6879(09)64011-8
62. Lipid Nanodiscs as a Tool for High-Resolution Structure Determination of Membrane Proteins by Single-Particle Cryo-EM. (2017). In *Methods in Enzymology* (Vol. 594, pp. 1–30). Academic Press. https://doi.org/10.1016/bs.mie.2017.05.007
63. Cheng, Y., Grigorieff, N., Penczek, P. A., & Walz, T. (2015). A Primer to Single-Particle Cryo-Electron Microscopy. *Cell*, *161*(3), 438–449. https://doi.org/10.1016/j.cell.2015.03.050
64. Fernandez-Leiro, R., & Scheres, S. H. W. (2016). Unravelling the structures of biological macromolecules by cryo-EM. *Nature*, *537*(7620), 339–346. https://doi.org/10.1038/nature19948
65. Kühlbrandt, W. (2014). The Resolution Revolution. *Science*, *343*(6178), 1443–1444. https://doi.org/10.1126/science.1251652
66. Beck, A., & Reichert, J. M. (2012). Marketing approval of mogamulizumab. *mAbs*, *4*(4), 419–425. https://doi.org/10.4161/mabs.20996

67. Mujić-Delić, A., Wit, R. H. de, Verkaar, F., & Smit, M. J. (2014). GPCR-targeting nanobodies: Attractive research tools, diagnostics, and therapeutics. *Trends in Pharmacological Sciences*, *35*(5), 247–255. https://doi.org/10.1016/j.tips.2014.03.003
68. Bao, G., Tang, M., Zhao, J., & Zhu, X. (2021). Nanobody: A promising toolkit for molecular imaging and disease therapy. *EJNMMI Research*, *11*(1), 6. https://doi.org/10.1186/s13550-021-00750-5
69. Jovčevska, I., & Muyldermans, S. (2020). The Therapeutic Potential of Nanobodies. *BioDrugs*, *34*(1), 11–26. https://doi.org/10.1007/s40259-019-00392-z
70. Muyldermans, S. (2013). Nanobodies: Natural Single-Domain Antibodies. *Annual Review of Biochemistry*, *82*(1), 775–797. https://doi.org/10.1146/annurev-biochem-063011-092449
71. Steeland, S., Vandenbroucke, R. E., & Libert, C. (2016). Nanobodies as therapeutics: Big opportunities for small antibodies. *Drug Discovery Today*, *21*(7), 1076–1113. https://doi.org/10.1016/j.drudis.2016.04.003
72. Irobalieva, R. N., Manolaridis, I., Jackson, S. M., Ni, D., Pardon, E., Stahlberg, H., Steyaert, J., & Locher, K. P. (2023). Structural Basis of the Allosteric Inhibition of Human ABCG2 by Nanobodies. *Journal of Molecular Biology*, *435*(19), 168234. https://doi.org/10.1016/j.jmb.2023.168234
73. McMahon, C., Baier, A. S., Pascolutti, R., Wegrecki, M., Zheng, S., Ong, J. X., Erlandson, S. C., Hilger, D., Rasmussen, S. G. F., Ring, A. M., Manglik, A., & Kruse, A. C. (2018). Yeast surface display platform for rapid discovery of conformationally selective nanobodies.

Nature Structural & Molecular Biology, *25*(3), 289–296. https://doi.org/10.1038/s41594-018-0028-6

74. He, Y., Wang, K., & Yan, N. (2014). The recombinant expression systems for structure determination of eukaryotic membrane proteins. *Protein & Cell*, *5*(9), 658–672. https://doi.org/10.1007/s13238-014-0086-4
75. Bill, R. M., Henderson, P. J. F., Iwata, S., Kunji, E. R. S., Michel, H., Neutze, R., Newstead, S., Poolman, B., Tate, C. G., & Vogel, H. (2011). Overcoming barriers to membrane protein structure determination. *Nature Biotechnology*, *29*(4), 335–340. https://doi.org/10.1038/nbt.1833
76. Vieira Gomes, A. M., Souza Carmo, T., Silva Carvalho, L., Mendonça Bahia, F., & Parachin, N. S. (2018). Comparison of Yeasts as Hosts for Recombinant Protein Production. *Microorganisms*, *6*(2), 38. https://doi.org/10.3390/microorganisms6020038
77. Nielsen, J. (2013). Production of biopharmaceutical proteins by yeast. *Bioengineered*, *4*(4), 207–211. https://doi.org/10.4161/bioe.22856
78. Chloupková, M., Pickert, A., Lee, J.-Y., Souza, S., Trinh, Y. T., Connelly, S. M., Dumont, M. E., Dean, M., & Urbatsch, I. L. (2007). Expression of 25 Human ABC Transporters in the Yeast Pichia pastoris and Characterization of the Purified ABCC3 ATPase Activity. *Biochemistry*, *46*(27), 7992–8003. https://doi.org/10.1021/bi700020m
79. Cereghino, J. L., & Cregg, J. M. (2000). Heterologous protein expression in the methylotrophic yeast Pichia pastoris. *FEMS Microbiology Reviews*, *24*(1), 45–66. https://doi.org/10.1111/j.1574-6976.2000.tb00532.x

80. le Maire, M., Champeil, P., & Møller, J. V. (2000). Interaction of membrane proteins and lipids with solubilizing detergents. *Biochimica et Biophysica Acta (BBA) - Biomembranes, Detergents in Biomembrane Studies*, *1508*(1), 86–111. https://doi.org/10.1016/S0304-4157(00)00010-1
81. Seddon, A. M., Curnow, P., & Booth, P. J. (2004). Membrane proteins, lipids and detergents: Not just a soap opera. *Biochimica et Biophysica Acta (BBA) - Biomembranes, Lipid-Protein Interactions*, *1666*(1), 105–117. https://doi.org/10.1016/j.bbamem.2004.04.011
82. Alexander, C. G., Wanner, R., Johnson, C. M., Breitsprecher, D., Winter, G., Duhr, S., Baaske, P., & Ferguson, N. (2014). Novel microscale approaches for easy, rapid determination of protein stability in academic and commercial settings. *Biochimica et Biophysica Acta*, *1844*(12), 2241–2250. https://doi.org/10.1016/j.bbapap.2014.09.016
83. Punjani, A., Rubinstein, J. L., Fleet, D. J., & Brubaker, M. A. (2017). cryoSPARC: Algorithms for rapid unsupervised cryo-EM structure determination. *Nature Methods*, *14*(3), 290–296. https://doi.org/10.1038/nmeth.4169
84. D'Imprima, E., Floris, D., Joppe, M., Sánchez, R., Grininger, M., & Kühlbrandt, W. (2019). Protein denaturation at the air-water interface and how to prevent it. *eLife*, *8*, e42747. https://doi.org/10.7554/eLife.42747
85. *E. coli Extract Polar | Avanti Research*. (n.d.). Retrieved August 24, 2026, from https://www.avantiresearch.com/en-gb/products/product/100600-e-coli-extract-polar
86. Grau-Campistany, A., Strandberg, E., Wadhwani, P., Reichert, J., Bürck, J., Rabanal, F., & Ulrich, A. S. (2015). Hydrophobic mismatch demonstrated for membranolytic peptides

and their use as molecular rulers to measure bilayer thickness in native cells. *Scientific Reports*, *5*(1), 9388. https://doi.org/10.1038/srep09388

87. Johansen, N. T., Tidemand, F. G., Nguyen, T. T. T. N., Rand, K. D., Pedersen, M. C., & Arleth, L. (2019). Circularized and solubility-enhanced MSPs facilitate simple and high-yield production of stable nanodiscs for studies of membrane proteins in solution. *The FEBS Journal*, *286*(9), 1734–1751. https://doi.org/10.1111/febs.14766
88. Flayhan, A., Mertens, H. D. T., Ural-Blimke, Y., Martinez Molledo, M., Svergun, D. I., & Löw, C. (2018). Saposin Lipid Nanoparticles: A Highly Versatile and Modular Tool for Membrane Protein Research. *Structure(London, England:1993)*, *26*(2), 345-355.e5. https://doi.org/10.1016/j.str.2018.01.007
89. Carlson, M. L., Young, J. W., Zhao, Z., Fabre, L., Jun, D., Li, J., Li, J., Dhupar, H. S., Wason, I., Mills, A. T., Beatty, J. T., Klassen, J. S., Rouiller, I., & Duong, F. (n.d.). The Peptidisc, a simple method for stabilizing membrane proteins in detergent-free solution. *eLife*, *7*, e34085. https://doi.org/10.7554/eLife.34085